A Numerical Study of Finite Element Calculations for Incompressible Materials under Applied Boundary Displacements

A Thesis

Submitted to the College of Graduate Studies and Research

in Partial Fulfillment of the Requirements

for the Degree of

Master of Science

in

the Department of Mechanical Engineering

by

Vinay Kumar Nagarkal VenkataKrishnaiah

© Copyright Vinay Kumar Nagarkal, August 2006. All rights reserved

Permission to Use

In presenting this thesis in partial fulfillment of the requirements for a Master of Science degree from the University of Saskatchewan, I agree that the Libraries of this University may make it freely available for inspection. I further agree that permission for copying this thesis in any manner, in whole or in part, for scholarly purposes, may be granted by the professors who supervised my thesis work or, in their absence, by the Head of the Department or Dean of the College in which my thesis work was done. It is understood that any copying, publication or use of this thesis or parts thereof for financial gain shall not be allowed without my written permission. It is also understood that due recognition shall be given to me and to the University of Saskatchewan in any scholarly use which may be made of any material in my thesis.

Requests for permission to copy or to make other use of material in this thesis, in whole or in part should be addressed to:

Head of the Department of Mechanical Engineering

University of Saskatchewan

Engineering Building

57 Campus Drive

Saskatoon, Saskatchewan, S7N 5A9

Canada

Abstract

In this thesis, numerical experiments are performed to test the numerical stability of the finite element method for analyzing incompressible materials from boundary displacements. The significance of the study relies on the fact that incompressibility, or density preservation during deformation, is an important property of materials such as rubber and soft tissue.

It is well known that the finite element analysis (FEA) of incompressible materials is less straightforward than for materials which are compressible. The FEA of incompressible materials using the usual displacement based finite element method results in an unstable solution for the stress field. Hence, a different formulation called the mixed u-p formulation (u– displacement, p – pressure) is used for the analysis. The u-p formulation results in a stable solution but only when the forces and/or stress tractions acting on the structure are known. There are, however, certain situations in the real world where the forces or stress tractions acting on the structure are unknown, but the deformation (i.e. displacements) due to the forces can be measured. One example is the stress analysis of soft tissues. High resolution images of initial and deformed states of a tissue can be used to obtain the displacements along the boundary. In such cases, the only inputs to the finite element method are the structural geometry, material properties, and boundary displacements. When finite element analysis of incompressible materials with displacement boundary conditions is performed, even the mixed u-p formulation results in highly unstable calculations of the stress field. Here, a hypothesis for solving this

problem is developed and tested. Theories of linear and nonlinear stress analysis are reviewed to demonstrate that it may be possible to determine the von Mises stress uniquely in spite of the numerical instability inherent in the calculations.

To validate this concept, four different numerical examples representing different deformation processes are considered using ANSYS®: a plate in simple shear; expansion of a thick-walled cylinder; a plate in uniform strain; and Cook's membrane. Numerical results show that, unlike the normal stress components σ_x, σ_y, and σ_z, the calculated values of the von Mises stress are reasonably accurate if measurement errors in the displacement data are small. As the measurement error increases, the error in the von Mises stress increases approximately linearly for linear problems, but can become unacceptably large in nonlinear cases, to the point where solution process encounter fatal errors. A quasi-Dirichlet patch test in association with this problem is also introduced.

Acknowledgements

I would like to express my sincere gratitude to my supervisors, Dr. Allan Dolovich and Dr. Reza Fotouhi for their invaluable guidance and encouragement throughout the entire process of this research work. I wish to extend my acknowledgement to Ms. L.M. Coley for sharing many technical details discussed in this thesis.

I would like to take this opportunity to appreciate the advisory committee members Dr. J.D. Bugg and Dr. W.J. Zhang for their suggestions and feedback.

I would also like to sincerely thank the Department of Mechanical Engineering for providing financial support in the form of Graduate Teaching Fellowships.

Table of Contents

CHAPTER 4 - NUMERICAL RESULTS

List of Figures

List of Tables

Nomenclature

$\boldsymbol{\sigma}$	Stress state at a point
$\boldsymbol{\sigma}_{volumetric}$	Volumetric component of stress
$\boldsymbol{\sigma}_{deviatoric}$	Deviatoric component of stress
P	Hydrostatic pressure
σ_x	Normal stress component along the X coordinate
σ_y	Normal stress component along the Y coordinate
σ_z	Normal stress component along the Z coordinate
τ_{xy}	Shear stress along the x-y plane
τ_{yz}	Shear stress in the y-z plane
τ_{zx}	Shear stress in the z-x plane
γ_{xy}	Shear strain in the x-y plane
γ_{yz}	Shear strain in the y-z plane
γ_{zx}	Shear strain in the z-x plane
σ_{eqv}	von Mises stress
ν	Poisson's ratio of the material
E	Young's modulus of the material
$u_{i,j}$	The partial derivative of the i^{th} component of displacement with respect to the j^{th} coordinate direction

ε_{ij}	Strain tensor components
D_{ijkl}	Elastic modulus tensor containing elastic constants, E and ν
B_i	Body forces
a_i	A prescribed displacement component
T_i	Prescribed stress traction
n_i	Direction cosines of the unit normal to the surface
Γ_1, Γ_2	Regions on the boundary
F	Deformation gradient tensor
W	Strain energy potential
C	Cauchy-Green deformation tensor
E	Green-Lagrange strain tensor
S	Second Piola-Kirchoff stress tensor
X_i	Coordinates of a point in the initial configuration
x_i	Coordinates of a point in the deformed configuration.
J	Jacobian
R_{ij}	Orthogonal tensor representing rigid body rotation
U_{ij}	The right stretch tensor, a symmetric tensor which contains the information on the stretches in the principal directions
δ_{ij}	Kronecker delta
C_i	Mooney – Rivlin constants to be determined experimentally
λ_1 ,λ_2 ,λ_3	Three principal stretches

π	Potential energy
[K]	The global stiffness matrix
{u}	Displacement vector
{f}	Force vector
K_{uu}	A symmetric and positive definite matrix of the order equal to the total number of unrestrained nodal degrees of freedom of the system
K_{up}	A matrix that enforces the incompressibility constraint on the system
N_U	Number of equilibrium equations
N_p	Number of volumetric constraint equations
C	Count condition
α	Shear Factor, a measure of deformation
r	Random number
U_i	Displacement without error at node i
u_i	Displacement with error at node i
e_{max}	Maximum error in displacement
Q4P1	Four node bilinear quadrilateral element with constant pressure interpolation

Chapter 1

Introduction

1.0 Incompressible Materials

Soft tissues and rubber are good examples of incompressible or nearly incompressible materials. The term incompressible means these materials cannot be triaxially compressed i.e. there is no change in volume due to deformation. To illustrate this concept, the following two deformation processes are considered. Consider a rubber block subjected to pressure, P, on all six faces as shown in Figure 1. Under this symmetric loading, conservation of the block's volume dictates that irrespective of the value of P, there is no deformation. This is referred to as the incompressible behaviour of the material.

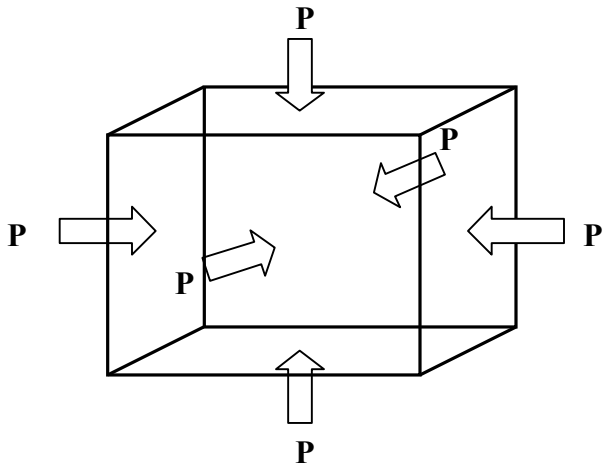

Figure 1: A Rubber Block Loaded Symmetrically with Pressure P on All Six Faces

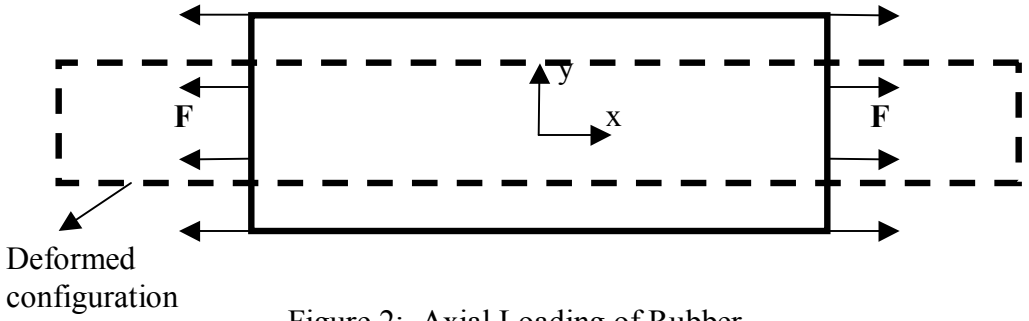

Figure 2: Axial Loading of Rubber

Now, consider a rectangular section of rubber subjected to a net tensile force, F, as shown in Figure 2. The deformation in this case would be such that the elongation in the x direction results in a reduction in the dimensions in the y and z directions sufficient to preserve the original volume of the material. Hence, for an incompressible material, the change in volume is zero when deformed, irrespective of the type and magnitude of loading. In addition, the volumetric strain, ε_V, defined as the ratio of change in volume to the original volume is also zero. The fact that a material is incompressible results in some important properties. In the case of isotropy, the Poisson's ratio, ν, is equal to one-half. Incompressible elastic materials in general also have the ability to undergo large elastic deformations without a permanent set and are usually modeled as hyperelastic, with linear or nonlinear stress – strain relationships.

1.1 Finite Element Analysis of Incompressible Materials

It is often necessary to perform stress analysis of soft tissues, rubber or other industrial materials that are modeled as incompressible. The finite element method (FEM) is a

robust numerical technique that can be used to obtain approximate solutions to these problems. Stress analysis of incompressible materials using the finite element method, however, is not straightforward. The usual displacement based finite element method is robust for most problems, but encounters difficulties when incompressible materials are analyzed [1]-[3]. As the value of ν approaches one-half, the final system of equilibrium equations becomes highly ill-conditioned resulting in a loss of solution accuracy. Hence, a different formulation called the mixed u-p formulation (u – displacement, p – pressure) is used for the analysis of incompressible materials. One requirement of the mixed u-p finite element method in order to obtain a stable solution is that the forces and/or stress tractions must be specified at some point on the structural boundary. There are, however, certain situations in the real world where the forces or stress tractions acting on the structure are unknown, but the deformation (displacements) due to these forces is known. In such a case, the final system of equations of the mixed u-p method becomes highly ill-conditioned resulting in a loss of solution accuracy similar to the displacement based FEM. The current work focuses mainly on this issue.

1.2 Objective

The current research project serves as a preliminary study towards the long-term goal of using the conventional displacement and mixed u-p finite element methods to model soft tissues using the displacement data obtained from high-resolution images [29]. To achieve this goal, it is very important to first understand the performance of these

methods under prescribed boundary displacements and the incompressibility condition. Therefore, the objective of the current work is,

"To numerically investigate the performance of the displacement based and the mixed u-p finite element methods, when stress analysis of incompressible materials is performed by prescribing the displacements along the boundary".

1.3 Scope of the Project

It is a well known fact that FEM systems of equations become highly ill-conditioned, resulting in multiple non-trivial solutions for stresses when displacements are the only prescribed quantities on the boundary. In References [4] to [6] this problem has been briefly discussed, but in the physical sense only. To the best of the author's knowledge, there is no published literature that extensively studies the behaviour of the conventional finite element method when incompressible materials are analyzed by prescribing boundary displacements. According to References [4] to [6] it appears that this problem is considered to be that of the underdetermined type, where no unique solution is possible. It will be shown here, however, that the final system of equations is partially underdetermined and partially exactly-determined; that is, some of the important stress components, namely the deviatoric component of stress and the von Mises stress, can be uniquely and accurately determined from these ill-conditioned systems of equations. The main focus of this study is on numerical instability and the behaviour of the ill-conditioned final systems of equations emerging during finite element analysis. The

commercial finite element package ANSYS® is used to carry out the numerical simulations. Both linear and nonlinear incompressible elastic cases are considered for the study. The displacement based finite element method is used to model linear elastic materials, whereas the mixed u-p finite element method is used with a hyperelastic constitutive law.

1.4 Thesis Organization

The organization of the later chapters of the thesis is discussed here. A brief and conclusive coverage of the background theory required to clearly demonstrate the problem considered in the current work is presented in Chapter 2. Various concepts of linear and nonlinear continuum mechanics used in solving structural problems are first discussed, followed by the basics of the finite element method and different formulations used in the current work. In Chapter 3, the difficulties encountered during the stress analysis of incompressible materials with prescribed boundary displacements and a hypothesis for possible solution are presented in detail. Chapter 4 of this thesis consists of results and discussions of the numerical simulations performed to test the hypothesis stated in Chapter 3. Four typical engineering test problems are considered. The results obtained by varying different parameters of the analysis are presented and discussed. Chapter 5 consists of the conclusions drawn based on the numerical results presented in Chapter 4 of the thesis followed by some recommendations for future work.

Chapter 2

Background Theory

2.0 Introduction

In this chapter, some basic equations used to solve boundary value problems in structural mechanics are reviewed. The discussion covers the general theories of linear elasticity and hyperelasticity, followed by the finite element formulations used in the current work. The entire discussion is within the realm of incompressible elastic materials.

2.1 Some Important Concepts

The deformation of any solid matter due to external forces can be decomposed into two components: the change in volume, and the distortion or change in shape, as shown in Figure 3.

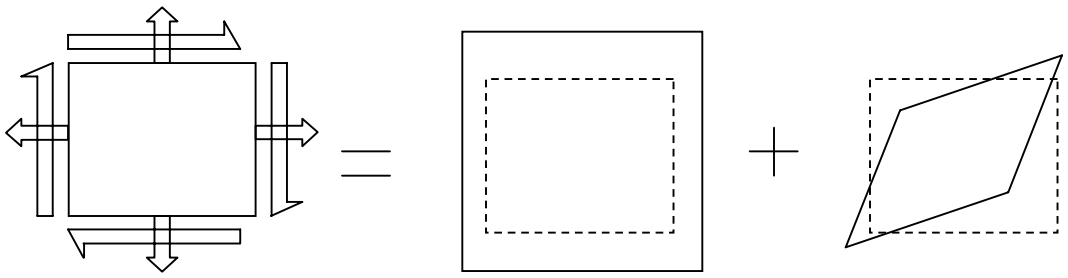

Figure 3: Decomposition of Deformation into (a) Change in Volume (b) Change in Shape

Similar to deformation, even stress and strain within the body can be decomposed into different components. It is usually convenient, especially for analysis of incompressible materials, to decompose the stress field into volumetric and deviatoric components. The volumetric component (mean stress or hydrostatic pressure) represents the stress developed within a body as a result of change in its volume, and the deviatoric component represents the internal stresses developed due to the distortion or change of shape.

Mathematically, the stress state, $\boldsymbol{\sigma}$, at any point can be decomposed as,

$$\boldsymbol{\sigma} = \boldsymbol{\sigma}_{\text{volumetric}} + \boldsymbol{\sigma}_{\text{deviatoric}} \quad (1)$$

[1]

where

$\boldsymbol{\sigma}$ = is the stress state at a point,

$\boldsymbol{\sigma}_{\text{volumetric}}$ = is the volumetric component of stress, and

$\boldsymbol{\sigma}_{\text{deviatoric}}$ = is the deviatoric component of stress.

In a three dimensional state of stress, the volumetric component, usually known as the hydrostatic pressure, P, is given by,

$$P = \frac{(\sigma_x + \sigma_y + \sigma_z)}{3} \quad (2)$$

where $\sigma_X, \sigma_Y, \sigma_Z$ [1] are the three normal stress components.

Therefore, the stress state at any point can be written as

$$\begin{bmatrix} \sigma_{xx} & \tau_{xy} & \tau_{xz} \\ \tau_{yx} & \sigma_{yy} & \tau_{yz} \\ \tau_{zx} & \tau_{zy} & \sigma_{zz} \end{bmatrix} = \begin{bmatrix} P & 0 & 0 \\ 0 & P & 0 \\ 0 & 0 & P \end{bmatrix} + \begin{bmatrix} \sigma_{xx} - P & \tau_{xy} & \tau_{xz} \\ \tau_{yx} & \sigma_{yy} - P & \tau_{yz} \\ \tau_{zx} & \tau_{zy} & \sigma_{zz} - P \end{bmatrix}. \quad (3)$$

[1] σ_X, σ_Y and σ_Z are same as σ_{xx}, σ_{yy} and σ_{zz}, the normal stress components.

2.2 Theory of Linear Elasticity

An isotropic material is said to be linear elastic if it obeys Hooke's law, that is the components of stress are linearly related to the components of strain within the elastic limit. To set the context for the fundamental concepts underlying the work in this thesis, an overview of some basic equations used to solve problems in the domain of linear elasticity is given in tensor notation, as follows.

Strain – displacement equations: $\varepsilon_{ij} = \frac{1}{2}\left(u_{i,j} + u_{j,i} \right)$ (4)

Stress – strain relation: $\sigma_{ij} = D_{ijkl}\,\varepsilon_{kl}$ (5)

Equilibrium equations: $\sigma_{ji,j} + B_i = 0$ (6)

Compatibility equations: $\varepsilon_{ij,kl} + \varepsilon_{kl,ij} - \varepsilon_{ik,jl} - \varepsilon_{jl,ik} = 0$ (7)

Boundary conditions: $u_i = a_i \text{ on } \Gamma_1$, essential or displacement boundary conditions (8)

$\sigma_{ij}\, n_j = T_i \text{ on } \Gamma_2$, natural or Force/stress traction boundary (9)

conditions

where

$u_{i,j}$ = the partial derivative of the i^{th} component of displacement with respect to the j^{th} coordinate direction,

ε_{ij} = the strain tensor components,

D_{ijkl} = the elastic modulus tensor containing elastic constants, E and ν,

σ_{ij} = the stress tensor components,

B_i = the body forces,

a_i = a prescribed displacement component,

T_i = a prescribed stress traction,

n_i = the direction cosines of the unit normal to the surface, and

Γ_1 and Γ_2 = regions on the boundary Γ.

2.3 Theory of Hyperelasticity

The theory discussed in Section 2.2 is valid only for small strain problems and where the relationship between stress and strain is linear. Incompressible materials like soft tissues and rubber can be seldom modeled as linear elastic. The relationship between stress and strain is usually nonlinear (known as material nonlinearity) and the material has the ability to undergo very large deformations (known as geometric nonlinearity). One effective way of dealing with both material and geometric nonlinearities of incompressible elastic materials is to model the material as hyperelastic.

A material is said to be hyperelastic [7] if there exists a strain energy potential, W, which is a scalar function of the deformation tensor, C_{ij}, and whose derivative with respect to a strain component, E_{ij}, determines the corresponding stress component, S_{ij}.

That is, for a hyperelastic material, $$S_{ij} = \frac{\partial W}{\partial E_{ij}} \quad . \tag{10}$$

The following discussion briefly outlines the mathematical theory of hyperelasticity, as discussed in [8].

2.3.1 Deformation Gradient

The fundamental quantity used to define the deformation of a body in finite strain analyzes is the deformation gradient tensor **F**. Consider a material vector d**X** which, under loading, becomes d**x** in the deformed configuration as shown in Figure 4.

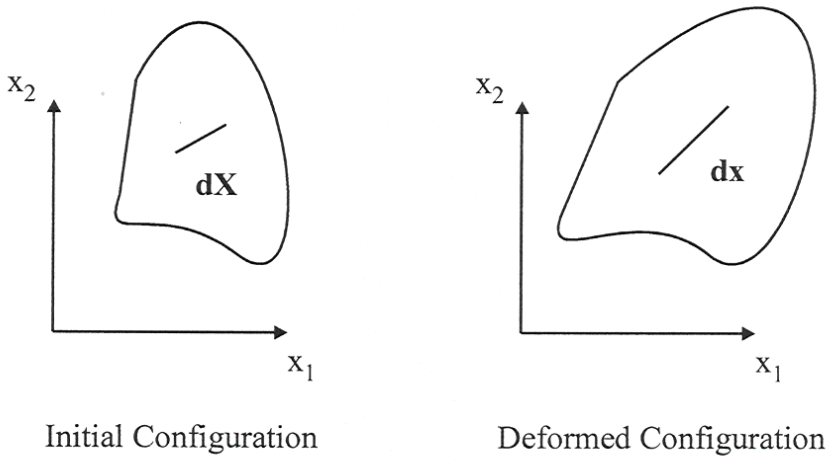

Figure 4: Initial and Final Configurations of a Hyperelastic Body

By calculus, the relationship between $d\mathbf{X}$ and $d\mathbf{x}$ is given by

$$d\mathbf{x} = \mathbf{F}\, d\mathbf{X}, \tag{11}$$

where **F** is the deformation gradient tensor and is defined by

$$F_{ij} = \frac{\partial x_i}{\partial X_j} \tag{12}$$

where

X_i = coordinates of a point in the initial configuration, and

x_i = coordinates of a point in the deformed configuration.

The deformation gradient is a tensor that describes the deformation of a material vector. It does not have any information on translation, but contains information on the stretches in the principal directions and rigid body rotation of the material vector. The determinant of the deformation gradient represents the change in volume in terms of the Jacobian, J.

$$dv = J\,dV; \quad J = \det \mathbf{F} \tag{13}$$

The Jacobian, J, is equal to unity for perfectly incompressible materials as the final volume (dv) is equal to the initial volume (dV). Similar to the stress field decomposition discussed in Section 2.1, even the deformation gradient can be decomposed into deviatoric and volumetric components as,

$$\mathbf{F} = J^{1/3}\,\hat{\mathbf{F}} \tag{14}$$

where

$J^{1/3}\,\mathrm{I}$ = the volumetric component, and

$\hat{\mathbf{F}}$ = the deviatoric component of the deformation gradient.

For a perfectly incompressible material, $\mathbf{F} = \hat{\mathbf{F}}$ as J = 1.

Using the polar decomposition theorem, the deformation gradient **F** can be decomposed as

$$F_{ij} = R_{ik}\,U_{kj} \tag{15}$$

where

R_{ij} = is an orthogonal tensor representing rigid body rotation, and

U_{ij} = the right stretch tensor, a symmetric tensor which contains information on the stretches in the principal directions.

2.3.2 Right Cauchy - Green Deformation Tensor

In order to obtain the stretch tensor so that the stretches in the principal directions can be calculated, the Cauchy – Green deformation tensor, **C**, is evaluated. As the deformation gradient consists of stretches as well as rigid body rotations of the material vector, it is necessary to eliminate the rigid body rotations so that the stretches of the material vector can be calculated. Hence, the right Cauchy – Green deformation tensor is defined as,

$$\mathbf{C}=\mathbf{F}^{\mathbf{T}}\mathbf{F} \ . \tag{16}$$

From equation (15), $$\mathbf{C}=\mathbf{U}^{\mathbf{T}}\mathbf{R}^{\mathbf{T}}\mathbf{R}\mathbf{U}, \tag{17}$$

so $$\mathbf{C}=\mathbf{U}^{\mathbf{2}}. \tag{18}$$

Upon eigenvalue decomposition of the stretch tensor **U**, the principal stretches, $\lambda_1, \lambda_2, \lambda_3$ and principal directions can be determined.

2.3.3 Green – Lagrange Strain Tensor

The usual definition of strain given by equation (4) holds for only infinitesimal strains. When it comes to finite strain analyzes, strain within the body is usually defined in terms of the stretch tensor. The most commonly used measure of strain in finite strain analyzes is the Green's strain, **E**, defined as,

$$E_{ij} = \frac{1}{2}\left(C_{ij} - \delta_{ij}\right) \tag{19}$$

where

δ_{ij} = the Kronecker delta.

2.3.4 Constitutive Law – Strain Energy Density Function

Strain energy is the energy stored in a body by virtue of an elastic deformation. Strain energy per unit deformed volume is known as strain energy density. In the case of hyperelasticity, the constitutive law is usually defined by a strain energy density function written in terms of the invariants of the deformation tensor, **C**. Some of the most popular and widely used hyperelastic strain energy functions are the Mooney – Rivlin model, the Neo-Hookean Model, the Ogden potential, and the Arruda-Boyce model [5]. In the current work, the Mooney - Rivlin material model is used for hyperelastic analyzes. This originates from the work by Mooney [9] and Rivlin [10]. This is one of the most widely used hyperelastic material models for practical applications.

2.3.4.1 Mooney – Rivlin Hyperelastic Material Model

A Mooney – Rivlin material is an isotropic, incompressible, hyperelastic material and is defined by,

$$W = C_1(I_1 - 3) + C_2(I_2 - 3) + C_3(I_1 - 3)^2 + C_4(I_1 - 3)(I_2 - 3) + C_5(I_2 - 3)^2 + \ldots, \tag{20}$$

where

C_i = Mooney – Rivlin constants to be determined experimentally,

I_1 = First invariant of $\mathbf{C} = \lambda_1^2 + \lambda_2^2 + \lambda_3^2$, and

I_2 = Second invariant of $\mathbf{C} = \lambda_1^2\lambda_2^2 + \lambda_2^2\lambda_3^2 + \lambda_3^2\lambda_1^2$.

Usually, 2 or 5 terms of the strain energy function given by equation (20) is used for most practical applications.

2.3.5 Stress Measure

Any quantity used as a measure of stress within a hyperelastic body must be work conjugate to the strain measure used to describe the strain in the material. A stress measure, **S**, is said to be work conjugate to a strain measure, **E,** if the product of stress, **S**, and change in strain, $\delta\mathbf{E}$, results in the actual change in strain energy per unit volume, δW ,of the deformed body. The stress measure that is work conjugate to Green's strain is the Second Piola – Kirchhoff stress, **S**, and is given by

$$S_{ij} = \frac{\partial W}{\partial E_{ij}} = 2\frac{\partial W}{\partial C_{ij}}. \tag{21}$$

The second Piola Kirchhoff stress can be decomposed into volumetric and deviatoric components as,

$$S_{ij} = 2\frac{\partial \hat{W}}{\partial C_{ij}} + P\,J\left[\mathbf{C}^{-1}\right]_{ij} \tag{22}$$

where

P = is the hydrostatic pressure, and

$\hat{W}$ = the distortional component of the strain energy potential.

The Second Piola – Kirchhoff stress, **S**, is a quantity that is contrived in order to satisfy the work conjugacy requirement and does not have a physical significance. Therefore, it must be converted into a physically meaningful true stress measure, such as the Cauchy (true) stress, $\boldsymbol{\sigma}$. The transformation used to achieve this is known as the Piola transformation and is given by

$$\boldsymbol{\sigma} = J^{-1}\mathbf{F}\mathbf{S}\mathbf{F}^{T} \tag{23}$$

Therefore,
$$\sigma_{ij} = 2F_{ik}\frac{\partial \hat{W}}{\partial C_{kl}}F_{jl} + P\delta_{ij} \tag{24}$$

where

I = the identity matrix,

and the hydrostatic pressure P must be evaluated from force and/or stress traction boundary conditions.

2.4 Finite Element Method

The classical differential equations become very difficult to solve in boundary value problems with complex geometries and loading conditions. This dictates the use of a numerical approach to obtain an approximate solution. The finite element method (FEM) [11] to [14] is one of the most important developments of numerical analysis. It is very

powerful for solving a wide variety of engineering problems. In FEM, the entire continuum is discretized into smaller units of finite size called 'elements' and the connecting points of adjacent elements are called 'nodes'. The field variables over each element are approximated using algebraic expressions known as shape functions. Hence, the governing equations of FEM are algebraic instead of differential equations in contrast to the classical analytical solution. Depending on the type of field variables used in the formulation, different names are used for different finite element formulations like, displacement (u), mixed u-p (u, p) and hybrid (σ, ε, u). In the following sections, the mathematical formulations of the displacement based FEM and the mixed u-p FEM used in the current work are discussed.

2.4.1 Displacement Based Finite Element Method

The displacement based FEM [11] to [14] is commonly formulated using the principle of stationary (or minimum) potential energy. The unknown field variables in this method are the nodal displacements, and hence the name displacement based FEM.

The principle of minimum potential energy is given by,

$$\text{Potential energy}\,(\pi) = \text{Strain Energy}\,(U) + \text{Work Potential}\,(\Omega)\,.$$

That is, for linear elasticity in the absence of body forces,

$$\pi = \frac{1}{2}\int_{\text{volume}} \{\sigma\}^T \{\varepsilon\} dv - \{u\}^T \{f\}\,. \tag{25}$$

By substituting equation (5) into equation (25),

$$\pi = \frac{1}{2}\int_{\text{volume}} \{\varepsilon\}^T [D] \{\varepsilon\} dv - \{u\}^T \{f\} \tag{26}$$

where $\{\sigma\}$, $\{\varepsilon\}$ and $\{f\}$ are the vectors containing the components of stress, strain and force respectively.

Considering the stationary condition of the functional (26) results in the final system of equations of the form,

$$[K]\ \{u\} = \{f\} \qquad (27)$$

where

[K] = the global stiffness matrix, which represents the stiffness of the discretized finite element model.

The displacement field {u} obtained by solving the equations (27) can be used with equations (4) to (7) to calculate the strain and stress values over the entire continuum.

2.4.2 Mixed u-p Finite Element Method

The displacement based FEM discussed in Section 2.4.1 is a very robust and widely used formulation. This method experiences problems, however, with the accurate calculation of the hydrostatic pressure, P, and hence the entire stress field, σ, when incompressible materials are analyzed. The problems encountered will be demonstrated in detail in Chapter 3 of this thesis. In order to overcome the problem with accurate calculation of the stress field, a different formulation called the mixed u-p formulation [11] is used. In this method, the hydrostatic pressure, P, is removed from the constitutive law given by equations (5) or (21), and is calculated as an unknown field variable along with the nodal displacements, u. Hence, this formulation is referred to as the mixed u-p FEM. The variational principle given by equation (26) is modified to achieve this. The mixed

formulation FEM mainly originates from the work by Herrmann [15] and other researchers [16] to [20]. The variational principle is modified by writing the potential energy functional similar to equation (26), except that the strain energy is expressed in terms of the deviatoric component only [16] – [20] and the incompressibility constraint is explicitly enforced by using a method such as the Lagrange multiplier method [21]. Hence the final system of finite element equations contains nodal displacements and Lagrange multipliers as unknowns, wherein the Lagrange multipliers turn out to be the hydrostatic pressure values within each element.

The modified potential energy functional is written as,

$$\pi(u,p) = \hat{\pi}(u) + \int_{Volume} \lambda(J-1)\, dV, \tag{28}$$

where, $\hat{\pi}(u)$ is the potential energy formulated in terms of the deviatoric component only and is given as

$$\hat{\pi}(u) = \int_{Volume} \hat{W}\, dV - \{u\}^T \{f\}. \tag{29},$$

where

$\hat{W}$ = is the deviatoric component of the strain energy density function, and

λ = the Lagrange multiplier.

The stationary condition of the functional (28) leads to the system of equations of the form

$$\begin{bmatrix} K_{uu} & K_{up} \\ K^T_{up} & 0 \end{bmatrix} \begin{Bmatrix} u \\ p \end{Bmatrix} = \begin{Bmatrix} f \\ 0 \end{Bmatrix}. \tag{30}$$

This results in the equations,

$$[K_{uu}]\{u\}+[K_{up}]\{p\}=\{f\}, \tag{31}$$

and

$$[K_{up}]^T\{u\}=\{0\} \tag{32}$$

where

K_{uu} = is a symmetric and positive definite matrix of the order equal to the total number of unrestrained nodal degrees of freedom of the system, and

K_{up} = is the matrix that enforces the incompressibility constraint on the system.

The set of equations given by (31) and (32) are the equilibrium and volumetric constraint equations, respectively.

2.5 Convergence of Finite Element Solution – Patch Test

The term 'convergence' in the context of finite element analysis means that the numerical solution approaches the exact solution as the approximation tends to zero. One method of reducing the approximation of the finite element grid is reducing the element size. This is referred to as the H – type [12] convergence of the finite element solution ('H' stands for element edge length). In order to verify if an element satisfies the requirements for convergence of the finite element solution, Irons [22] proposed a physical test known as the 'Patch test' for displacement based FEM. Later, this approach was extended to the mixed u-p FEM by Zienkiewicz et al [6]. In the current work, the element used for linear analyzes is a four node quadrilateral with displacement formulation. This element satisfies the patch test. In contrast, the element used for hyperelastic analyzes, a four node

quadrilateral with constant hydrostatic pressure (Q4P1) using mixed u-p formulation does not satisfy the patch test, and yet it is a widely used element [23].

2.5.1 Patch Test for Mixed u-p Formulation

For the mixed u-p formulation, a necessary condition (also known as the count condition 'C' [23]) to be satisfied for non-singularity of the system of equations (30) after application of boundary conditions is

$$N_U \geq N_P \tag{33}$$

or

$$\text{if } C = \frac{N_u}{N_P}, \text{ then } C \geq 1 \tag{34}$$

where

N_U = the number of equilibrium equations (31), which is equal to the total number of unrestrained nodal degrees of freedom and

N_p = the number of volumetric constraint equations, given by equation (32), which is equal to the total number of unknown pressure degrees of freedom.

A most severe Dirichlet patch test is achieved by fixing all the boundary displacements and specifying one pressure value [23]. In such a scenario, if any arbitrary patch of elements is capable of accurately representing a constant strain state with rigid body motions, and if the system of equations is non-singular, then the element is said to have passed the patch test. If such a test is performed on the patch of Q4P1 elements shown in Figure 5 then,

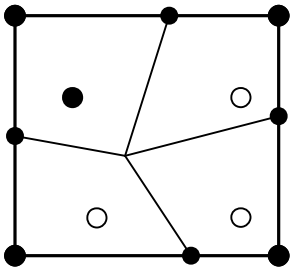

Figure 5: An Arbitrary Patch of Q4P1 Finite Elements

N_U = 2, as there are 2 internal nodal displacement degrees of freedom (at the common node for all the four elements) and N_p = 3, as there are only 3 unknown pressure values. Therefore, the count condition, C, is 2/3 and $C < 1$. Therefore, the necessary condition for convergence, equation (34), is violated and this element does not satisfy the patch test.

According to Hughes [23], if $C \leq 1$, there are more constraints than the available displacement degrees of freedom, hence, severe locking is to be expected. If the value of C is much greater than 2, then there are very few constraints to ensure the incompressibility behaviour of the finite element grid. Hence if,

$C > 2$, Too few incompressibility constraints

$C = 2$, Optimal

$C < 2$, Too many incompressibility constraints

$C \leq 1$, Locking

In this thesis these conditions are analyzed in accordance with the hypothesis discussed in Chapter 3.

2.6 Failure Criteria for Incompressible Materials

It is always important to predict the failure loads for various structural elements so that a better design can be achieved. Thus, a criterion for predicting the failure load in a structural element is of utmost importance. There are many failure criteria used depending on the type of material. For incompressible elastic materials, the commonly used failure criterion in the literature is the Maximum Distortion Energy theory, more popularly known as the von Mises criterion. According to this theory, at failure the energy causing distortion per unit volume is equal to the distortion energy per unit volume in a uniaxial state of stress at the elastic limit. The distortion energy per unit volume is closely related to the von Mises stress, given by,

$$\sigma_{eqv} = \frac{1}{\sqrt{2}}\left[(\sigma_x - \sigma_y)^2 + (\sigma_y - \sigma_z)^2 + (\sigma_z - \sigma_x)^2 + 6(\tau_{xy}^2 + \tau_{yz}^2 + \tau_{zx}^2)\right]^{1/2} \quad (35)$$

It is important to note that the calculation of the von Mises stress requires only the normal stress differences and the shear stress values. These together are the deviatoric components of stress, as these components contribute only to the change in shape or distortion of the structure.

Chapter 3

Problem Definition and Hypothesis

3.0 Introduction

In the case of incompressible analysis, a problem is said to be well posed if there is a unique solution satisfying the Dirichlet (displacement) and Neumann (force/stress traction) boundary conditions. If all the displacements along the boundary are prescribed and no force/stress traction is specified, such a problem is referred to as a Dirichlet problem. A Dirichlet problem of the incompressible case is an ill posed problem and hence does not have a unique solution. In this chapter, the difficulties encountered with the Dirichlet problem and possible solution are discussed.

3.1 Problem Description

3.1.1 Displacement Based FEM

Linear elastic isotropic materials are characterized by Young's modulus, E, and Poisson's ratio, ν. The constitutive relations of linear elastic isotropic materials for plane stress, plane strain and 3-D cases can be written, respectively as,

$$\begin{bmatrix}\sigma_x\\ \sigma_y\\ \tau_{xy}\end{bmatrix}=\frac{E}{1-\nu^2}\begin{bmatrix}1 & \nu & 0\\ \nu & 1 & 0\\ 0 & 0 & \frac{1-\nu}{2}\end{bmatrix}\begin{bmatrix}\varepsilon_x\\ \varepsilon_y\\ \gamma_{xy}\end{bmatrix} \tag{36}$$

$$\begin{bmatrix}\sigma_x\\ \sigma_y\\ \tau_{xy}\end{bmatrix}=\frac{E}{(1+\nu\ )(1-2\nu)}\begin{bmatrix}1-\nu & \nu & 0\\ \nu & 1-\nu & 0\\ 0 & 0 & \frac{1-2\nu}{2}\end{bmatrix}\begin{bmatrix}\varepsilon_x\\ \varepsilon_y\\ \gamma_{xy}\end{bmatrix} \tag{37}$$

$$\begin{bmatrix}\sigma_x\\ \sigma_y\\ \sigma_z\\ \tau_{xy}\\ \tau_{yz}\\ \tau_{zx}\end{bmatrix}=\frac{E}{(1+\nu)(1-2\nu)}\begin{bmatrix}1-\nu & \nu & \nu & 0 & 0 & 0\\ \nu & 1-\nu & \nu & 0 & 0 & 0\\ \nu & \nu & 1-\nu & 0 & 0 & 0\\ 0 & 0 & 0 & \frac{1-2\nu}{2} & 0 & 0\\ 0 & 0 & 0 & 0 & \frac{1-2\nu}{2} & 0\\ 0 & 0 & 0 & 0 & 0 & \frac{1-2\nu}{2}\end{bmatrix}\begin{bmatrix}\varepsilon_x\\ \varepsilon_y\\ \varepsilon_z\\ \gamma_{xy}\\ \gamma_{yz}\\ \gamma_{zx}\end{bmatrix} \tag{38}$$

These equations are of the form $\{\sigma\}=[D]\{\varepsilon\}$. The potential energy functional used in the displacement based FEM given by equation (26) includes the elasticity matrix [D], and so does the final system of equilibrium equations, [K]{u}={F}. It is known that the value of Poisson's ratio, ν, for perfectly incompressible materials is one-half. When ν = 0.5 is substituted into the above stress - strain relationships, the common multiplier of the elasticity matrices for the plane strain and 3-D cases goes to infinity, but not for the constitutive law for plane stress. This indicates that the displacement based FEM experiences problems during the analysis of perfectly incompressible materials for plane strain and 3-D problems. As a matter of numerical analysis, the value of ν can be

approximated to be very close to one – half, for example, $\nu = 0.49$, 0.499 or 0.4999… and so on. During such an approximation, the common multiplier of the matrix takes a finite value and hence the equilibrium equations can be solved to determine the unknown nodal displacements and hence strains and stresses within the body. Although the system of equations can be solved as a result of this approximation, it would lead to a system of equations which is ill-conditioned and hence unstable. In Table 1, the coefficient of the elasticity matrix for plane strain/3-D cases is calculated for three different values of Poisson's ratio to demonstrate the instability involved.

Table 1: Instability in the constitutive law

Poisson's ratio ν	Young's modulus E GPa	$\frac{E}{(1+\nu)(1-2\nu)}$ GPa
0.49	70	2348.99
0.499	70	23348.899
0.4999	70	233348.8899

From Table 1, it is evident that the common multiplier of the elasticity matrix and hence the equilibrium equations of the displacement based FEM for plane strain and 3-D problems is highly unstable for ν close to 0.5. This instability results in an inaccurate calculation of the hydrostatic pressure, P, when incompressible materials are analyzed. According to generalized Hooke's law, the constitutive relation for any linear isotropic material is given by,

$$\varepsilon_X = \frac{1}{E}\left[\sigma_X - \nu\sigma_Y - \nu\sigma_Z\right]$$
$$\varepsilon_Y = \frac{1}{E}\left[-\nu\sigma_X + \sigma_Y - \nu\sigma_Z\right] \qquad (39)$$
$$\varepsilon_Z = \frac{1}{E}\left[-\nu\sigma_X - \nu\sigma_Y + \sigma_Z\right],$$

where

$\varepsilon_X, \varepsilon_Y, \varepsilon_Z$ and $\sigma_X, \sigma_Y, \sigma_Z$ are the normal strains and stresses respectively.

From the theory of linear elasticity, it may be shown that the change in volume per volume (volumetric strain) of the material is given by,

$$\Delta V/V = (1+\varepsilon_X)(1+\varepsilon_Y)(1+\varepsilon_Z) - 1. \qquad (40)$$

Neglecting the higher order terms, equation (40) can be written as,

$$\Delta V/V \approx \varepsilon_X + \varepsilon_Y + \varepsilon_Z. \qquad (41)$$

Adding all three equations of (39),

$$\varepsilon_X + \varepsilon_Y + \varepsilon_Z = \frac{(1-2\nu)}{E}(\sigma_X + \sigma_Y + \sigma_Z). \qquad (42)$$

For linear isotropic materials, incorporating material incompressibility implies that $\varepsilon_X + \varepsilon_Y + \varepsilon_Z$ is approximately zero and $\nu \approx 0.5$. This results in an arbitrary value for the normal stress sum $(\sigma_X + \sigma_Y + \sigma_Z)$. Thus, the hydrostatic stress component, P, defined by

$$P = \frac{(\sigma_X + \sigma_Y + \sigma_Z)}{3} \qquad (43)$$

is indeterminate from known displacements and/or strains.

3.1.2 Mixed u-p FEM

To overcome the difficulties discussed in Section 3.1.1, the mixed u-p FEM is used for incompressible analysis of plane strain and 3-D problems. In this section it will be shown that when the mixed u-p FEM is used to solve a Dirichlet problem, it behaves in a similar fashion to the displacement based FEM.

In the case of the mixed u-p FEM (Section 2.4.2), the system of equations used to solve for the unknown nodal displacements, u, and hydrostatic pressure, P, is of the form,

$$\left[\begin{array}{c|c} K & B \\ \hline B^T & 0 \end{array}\right]\left[\begin{array}{c} u \\ \hline P \end{array}\right]=\left[\begin{array}{c} F \\ \hline 0 \end{array}\right]. \tag{44}$$

Now, this system of equations will be analyzed for a single Q4P1 element with prescribed boundary displacements as shown in Figure 6.

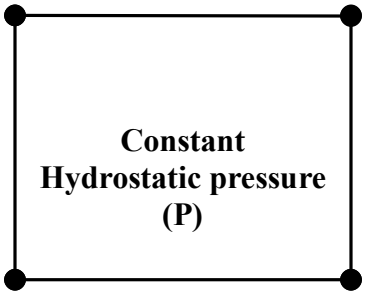

Figure 6: A Q4P1 Element with Prescribed Boundary Displacements

The Q4P1 element has four nodes with two translation degrees of freedom per node and one hydrostatic pressure, P, as the field variables. If all the displacements along the boundary are specified for this single element and analyzed for stresses, the unknowns

are eight nodal reaction forces and the hydrostatic pressure, P. Upon expansion, the system of equations (44) results in 9 equations of the form,

$$\left[\begin{array}{ccc|c} K_{11} & \cdots & K_{18} & b_1 \\ \vdots & \ddots & \vdots & \vdots \\ K_{81} & \cdots & K_{88} & b_8 \\ \hline b_1 & \cdots & b_8 & 0 \end{array}\right]\left[\begin{array}{c} u_1 \\ \vdots \\ v_4 \\ \hline p \end{array}\right]=\left[\begin{array}{c} F_1 \\ \vdots \\ F_8 \\ \hline 0 \end{array}\right], \tag{45}$$

or

$$\begin{aligned} F_1 - b_1 P &= K_{11}u_1 + \cdots\cdots + K_{18}u_8 \\ F_2 - b_2 P &= K_{21}u_1 + \cdots\cdots + K_{28}u_8 \\ &\vdots \\ F_8 - b_8 P &= K_{81}u_1 + \cdots\cdots + K_{88}u_8 \end{aligned} \tag{46}$$

and, $b_1u_1 + \cdots\cdots + b_8u_8 = 0$ (incompressibility constraint)

It is important to note that the last equation of (46) is nothing but the incompressibility condition and does not contain the term, P. Therefore, this equation does not provide any information in solving for the unknowns and hence, practically there are only 8 equations available to solve for 9 unknowns. Thus, at least one force value has to be specified on the boundary in order to solve this problem. If no force is specified, the value of hydrostatic pressure, P, becomes arbitrary. A similar pattern follows for a patch of more than one element; that is the number of unknowns is more than the number of available equations. Therefore, a unique and accurate hydrostatic pressure, P, cannot be determined

when all the boundary displacements are specified for an incompressible material modeled using the mixed u-p FEM.

3.2 A Possible Solution to the Problem

In this section, a possible remedy for the Dirichlet problem of the incompressible case is discussed. According to the literature [23], there are two possible methods for obtaining a unique solution to the Dirichlet problem when modeled using the mixed u-p FEM. They are as follows.

- The first method is to specify at least one hydrostatic pressure value in equation (44) which is used to solve for the unknown u and P values. Any arbitrary value of hydrostatic pressure results in an arbitrary value for normal stresses. It is the contention here that this is not a practically feasible solution for real world applications.
- The second possible solution methodology according to the literature is to specify a zero force on the boundary. This implies that a displacement value normal to the structural boundary at some node on the boundary is not specified. In such a case, the force at the node along that particular displacement direction is zero and this would reduce one unknown in the system of equations (44) and hence lead to a unique solution to the problem. This is a very convincing solution, but the zero force value has to be specified at a location where the force is zero in reality and not at any arbitrary location where there exists some force. The applications of the current work deal with displacement data from the images of soft tissues of living systems. In this scenario, it is difficult to know the exact zero force location, as the tissues are usually

surrounded by other tissues which might exert force on the tissue of interest. Hence, this solution becomes impractical for problems which are the target of the current work.

The proposed solution to the Dirichlet problem when modeled using the displacement based FEM and mixed u-p FEM will now be discussed.

As shown in Section 2.1, the stress state at any point within a body can be decomposed into hydrostatic and deviatoric components. Considering, for example, Hooke's law given by equation (39), it can be shown that [25]

$$\begin{aligned}
\sigma_x - \sigma_y &= \frac{E}{(1+\nu)}\left[\varepsilon_x - \varepsilon_y\right] \\
\sigma_y - \sigma_z &= \frac{E}{(1+\nu)}\left[\varepsilon_y - \varepsilon_z\right] \\
\sigma_z - \sigma_x &= \frac{E}{(1+\nu)}\left[\varepsilon_z - \varepsilon_x\right] \\
\tau_{xy} = \frac{E}{2(1+\nu)}\gamma_{xy}, \quad \tau_{yz} &= \frac{E}{2(1+\nu)}\gamma_{yz}, \quad \tau_{zx} = \frac{E}{2(1+\nu)}\gamma_{zx}.
\end{aligned} \tag{47}$$

From equation (47), it is evident that the normal stress differences and shear stress values can be determined from the constitutive law irrespective of the value of Poisson's ratio, ν. Fortuitously, the calculation of the von Mises stress given by equation (35) requires only the normal stress differences and shear stress values. Therefore, it can be concluded that when the displacement based FEM is used to analyze linear elastic isotropic incompressible materials with boundary displacement data, although the entire stress state cannot be uniquely determined, the deviatoric component of stress and hence the von Mises stress can be potentially determined if the numerical instability associated with the entire process does not prevent doing so.

3.3 Hypothesis

Based on the discussions in Sections 3.1 and 3.2 it can be hypothesized that,

"When the displacement based FEM or mixed u-p FEM is used to perform stress analysis of incompressible materials by prescribing the displacements along the boundary, it is not possible to accurately determine the hydrostatic pressure and thus the normal stresses. There is, however, enough information to overcome the numerical instability to accurately extract the deviatoric component of stress and hence the von Mises stress.

Therefore, the only possible solution to the Dirichlet problem of the incompressible case is to regard it as a problem for which only the deviatoric component of stress can be determined. This implies that the solution to such a problem involves a system of equations that is partially underdetermined where more than one solution is possible for the hydrostatic pressure, with the remaining part exactly determined where there exists a unique solution for the deviatoric component.

3.4 Effect of Error in Boundary Displacements

As shown in the previous sections, the system of equations for the Dirichlet problem of the incompressible case is ill-conditioned and hence unstable. This is a very important issue to be noted, as any small error in boundary displacements might result in a large error in the resulting stresses. When boundary displacements are measured using, for

example, an interferometer, there is always some error involved with the measured data. At this stage, although it is known that the deviatoric component of stress is theoretically obtainable, it is important to investigate if the error in the measured boundary displacements affects the uniqueness and stability of the resulting deviatoric component and hence the von Mises stress. This aspect is investigated with the aid of numerical examples in Chapter 4 of this thesis.

3.5 Convergence of von Mises Stress – Quasi Dirichlet Patch Test

An element in the context of the finite element method is said to be valid for practical applications if it has the ability to demonstrate numerical convergence. In the discussion of Section 2.6, it was noted that numerical convergence using the finite element method can be achieved only if the element passes the so called 'Patch test'. The Q4P1 element is very simple and easy to formulate and hence is widely used although this element does not satisfy the requirements of the Patch test. According to the hypothesis stated in Section 3.3, for incompressible Dirichlet problems it is possible to uniquely calculate only the deviatoric component of stress and hence the von Mises stress. Therefore, a modified patch test similar to the usual Dirichlet patch test, called the quasi Dirichlet patch test is introduced here[2]. To the best of the author's knowledge, a patch test similar to the quasi Dirichlet patch test has not been discussed in the literature. The purpose of this test is to evaluate the ability of the Q4P1 finite element to result in convergence of the deviatoric component of stress when used to solve the Dirichlet problem. In this test,

[2] This test was developed in collaboration with L.M. Coley

all the displacements along the boundary are specified for an arbitrary patch of elements and the von Mises stress is evaluated. The displacements are specified such that they correspond to a uniform von Mises stress field. In such a scenario, if a patch of elements has the ability to accurately represent a uniform field for von Mises stress then the element is said to have passed the quasi Dirichlet patch test. An element that passes the quasi Dirichlet patch test can be used for applications with all-displacement boundary conditions in order to calculate the von Mises stress.

Certain finite element grid configurations (shown in figure 8 (a), (b) and (c)) violate the count condition requirements of the actual patch test discussed in Section 2.5. It is intended in the current work to numerically investigate the effect of violation of the count condition on the calculated deviatoric component of stress. The count condition (C) [22] according to the quasi Dirichlet patch test for different finite element configurations is,

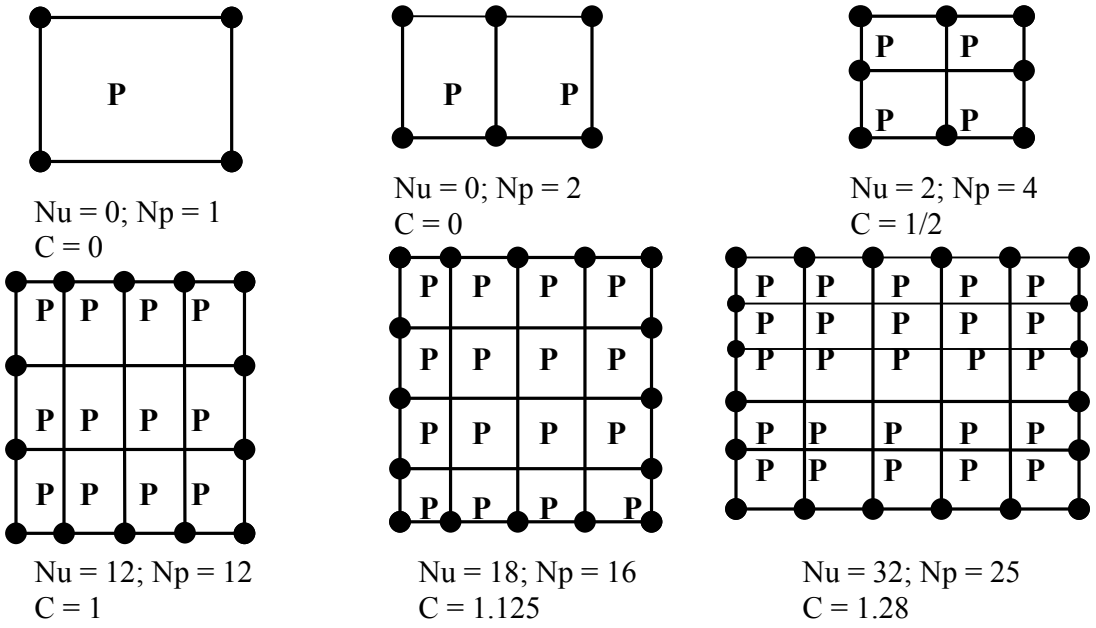

Figure 8: Count Condition for Different Patches of Q4P1 Elements

In the next chapter of this thesis, the numerical examples include the effect of count condition on the calculated values of von Mises stress.

Chapter 4

Numerical Results

4.0 Introduction

In this chapter, the hypothesis discussed in Chapter 3 is investigated with the aid of numerical examples. The commercial finite element package ANSYS® is used for numerical simulations. Four different test problems are considered:

1. A plate in simple shear;
2. Expansion of a thick walled cylinder;
3. A Plate in uniform strain; and
4. Cook's membrane.

The rationale behind the selection of these simple examples is that analytical solutions exist for most cases and these can be compared with the finite element results. Also, elementary fields such as these are normally used in the literature to test necessary conditions for numerical stability and convergence. Finally, some of these problems have relevance to actual problems in biomechanics. (Example: An artery can be modeled as expansion of a thick walled cylinder.) For cases where the analytical solution cannot be easily obtained, the results obtained by solving the problem using ANSYS® with force/stress traction boundary conditions is used as a reference for comparison.

4.1 A Plate in Simple Shear

The problem considered in this section is a plate in simple shear [26] for which the analytical solution can be easily obtained (See Appendix A). Figure 9 shows a plate in simple shear in its undeformed (solid line) and deformed (broken line) configurations.

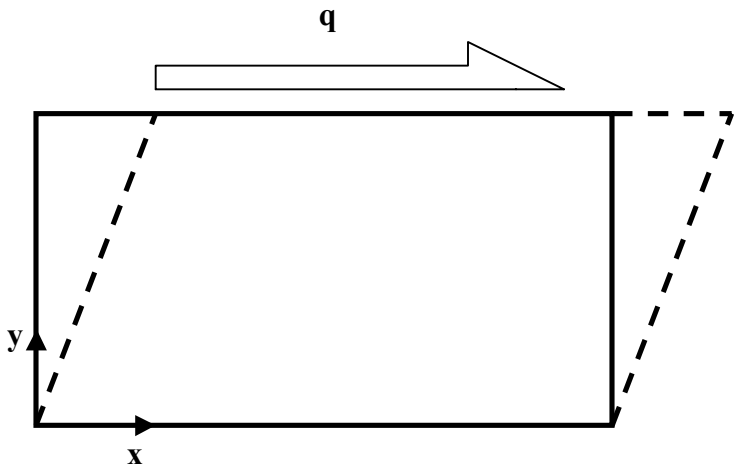

Figure 9: A Plate in Simple Shear

The mapping of coordinates in the initial and deformed configurations for this problem can be written as

$$\begin{aligned} x &= X + \alpha Y \\ y &= Y \\ z &= Z \end{aligned} \tag{48}$$

where

$X, Y, Z =$ are the coordinates of a material point in the initial configuration,

$x, y, z =$ are the coordinates of a material point in the deformed configuration, and

$\alpha =$ is the 'shear factor', a measure of deformation given as $\alpha = (x - X)/Y$.

4.1.1 Linear Elastic Analysis

For the linear elastic analysis, a very small value for the shear factor 'α' is chosen, namely $\alpha = 0.05$, and the stress-strain relationship is considered to be linear. The finite element model is generated using 4 node quadrilateral – displacement based elements. The Young's modulus, E, of the material is calculated as,

$$E = 6(C_1+C_2) \tag{49}$$

where

C_1 and C_2 are Mooney – Rivlin constants appropriate to model the hyperelastic behaviour of skin and are obtained from [27].

In this analysis, the effect of Poisson's ratio (discussed in Section 3.1) on the resulting stress field is numerically tested. Different values of Poisson's ratio close to the actual value of one-half are considered and the resulting stress values are reported in Table 2.

Analysis details:

- **Plate :** 0.1 m × 0.05 m
- **Boundary conditions:** Displacements 'u' and 'v' along the boundary are prescribed.
- **Material:** linear elastic material, E = 2040 Pa.
- **Element type:** Plane42 (4 node Quad) in plane strain (Displacement formulation).
- **Analysis type:** Small deformation - linear analysis.

Analytical Solution:

$\sigma_X = 841$ Pa, $\sigma_Y = 839$ Pa, $\sigma_Z = 840$ Pa and

$\sigma_{eqv} = 59.7$ Pa. (Obtained from nonlinear solution for $\alpha = 0.05$)

Table 2: FEM Solution for the Simple Shear case with α = 0.05

Poisson's ratio ν	σ_X [Pa]	σ_Y [Pa]	σ_Z [Pa]	σ_{eqv} [Pa]
$0.49_{[1]*}$	0.058E-11	0.085E-11	0.076E-11	59.2
$0.49_{[2]}$	-0.050E-10	-0.019E-10	- 0.035E-10	58.9
$0.49_{[3]}$	0.005E-08	- 0.001E-08	0.002E-08	58.8
$0.49_{[6]}$	-0.129E-06	- 0.136E-06	-0.132E-06	58.8
$0.49_{[8]}$	-0.062E-04	- 0.013E-04	- 0.037E-04	58.8

(* $\nu = 0.49_{[n]}$,the subscript 'n' represents numeral 9 repeating until the $(n+1)^{th}$ decimal place)

It can be seen from the above table that the normal stress values are highly unstable and hence unreliable. Although the system of equilibrium equations becomes ill-conditioned as the value of Poisson's ratio approaches one-half, the normal stress differences and shear stress values are still close to accurate values resulting in von Mises stress within an accuracy of 1.5%. Hence, the von Mises stress can be determined with reasonable accuracy using the displacement formulation finite elements under Dirichlet (displacement) boundary conditions (using ANSYS®).

4.1.1.1 Error Analysis

It is known that the system of equations becomes ill-conditioned as the Poisson's ratio approaches one-half, resulting in a significant amount of error in the solution for any small error in the input data. In this section, the effect of error in boundary displacement values on the resulting von Mises stress is studied. Two types of errors, constant errors

and random errors in boundary displacements are considered. This study determines the validity of the hypothesis in the case of error in the measured displacements.

4.1.1.1.1 Constant Error in Boundary Displacements

In this case, the same percentage error is added to the boundary displacements and the corresponding error in the resulting von Mises stress is tabulated in Table 3. It is evident from Table 2 that the normal stress values are not reliable even for exact values of the displacements. Therefore, only the von Mises stress, the stress component of interest, is reported.

Table 3: Error in von Mises stress due to constant displacement error

% Error in displacements	σ_{eqv} [Pa]	% Error in von Mises Stress
1	59.877	0.247
2	60.470	1.240
3	61.063	2.232
4	61.656	3.225

From Table 3 it is apparent that the constant error in the displacements does not have a significant impact on the error in von Mises stress in the case of this linear elastic analysis using the displacement based FEM.

4.1.1.1.2 Random Error in Boundary Displacements

In this section, random error in displacements along the boundary is considered. n random numbers (between 0 and 1) are generated for n nodes along the boundary and

each node is associated with a random number. Error in displacements at each node is incorporated as,

$$u_i = [(2r-1)e_{max} + 1]U_i \quad (50)$$

where, U_i and u_i = displacements without and with error at node i, and

r = the random number associated with node i, and

e_{max} = the maximum error in displacement.

Random numbers were generated for e_{max} = 1%, 2%, 3% and 4% and the corresponding displacements were calculated. Ten different sets of random errors were chosen for each level of error and the corresponding maximum errors in von Mises stress are reported. This gives an indication of the magnitude of error in the resulting von Mises stress due to random errors in the measured boundary displacements.

Analytical Solution: σ_{eqv} = 59.7 Pa (for displacements without error)

Table 4: Maximum displacement error of 1%

Random Set No	Maximum σ_{eqv} [Pa]	% Error in Maximum σ_{eqv}
1	59.427	-0.511
2	60.004	0.454
3	63.513	6.328
4	60.508	1.297
5	59.756	0.038
6	59.798	0.109
7	59.747	0.023
8	63.635	6.533
9	60.061	0.549
10	60.328	0.996

Table 5: Maximum displacement error of 2%

Random Set No	Maximum σ_{eqv} [Pa]	% Error in Maximum σ_{eqv}
1	60.432	1.171
2	61.876	3.588
3	62.740	5.033
4	61.661	3.228
5	61.527	3.004
6	60.892	1.940
7	63.730	6.691
8	63.645	6.549
9	63.310	5.989
10	62.849	5.221

Table 6: Maximum displacement error of 3%

Random Set No	Maximum σ_{eqv} [Pa]	% Error in Maximum σ_{eqv}
1	61.450	2.874
2	62.415	4.490
3	63.540	6.373
4	62.614	4.822
5	68.418	14.541
6	65.691	9.975
7	67.449	12.917
8	67.431	12.887
9	69.712	16.707
10	62.849	5.221

Table 7: Maximum displacement error of 4 %

Random Set No	Maximum σ_{eqv} [Pa]	% Error in Maximum σ_{eqv}
1	66.706	11.673
2	63.548	6.387
3	71.312	19.385
4	73.964	23.824
5	64.814	8.506
6	63.207	5.816
7	69.317	16.045
8	66.071	10.610
9	66.496	11.323
10	82.874	38.747

In the case of constant displacement errors, the error in the von Mises stress is approximately proportional to the error in the displacement data. In the case of random error in boundary displacements, however, the error in the von Mises stress varies in an indefinite manner. Also, the accuracy of the von Mises stress deteriorates rapidly with the increase in displacement error. In reality, any measured quantity is associated with constant and random errors. Thus, any method used to measure boundary displacements involves random errors which might lead to a highly inaccurate value of von Mises stress. Hence, it can be concluded that the accuracy of the measured displacements plays a very important role in the accuracy of the resulting von Mises stress.

4.1.2 Nonlinear Analysis

In this section, a nonlinear incompressible elastic material modeled as a Mooney- Rivlin hyperelastic material is considered for analysis and is subjected to large deformations by prescribing the displacements along the boundary. Deformation is increased by increasing the value of α in the mapping given by equation (48). Normal and von Mises stress values are reported in Table 8 for various deformation states. Both analytical (see appendix A) and FEM solutions are reported for comparison.

Analysis Details:

- **Plate :** 0.1 m × 0.05 m
- **Boundary conditions:** Displacements 'u' and 'v' along the boundary are prescribed.
- **Element type:** Hyper56 (Q4P1) – Mixed u-p formulation in plane strain.
- **Analysis type:** Large deformation - nonlinear analysis

The Mooney – Rivlin constants used to model hyperelastic behaviour are taken from [27]

Table 8: Stress state at large deformations

α	Type of Solution	σ_x [kPa]	σ_y [kPa]	σ_z [kPa]	σ_{eqv} [kPa]
0.5	FEM	0.338	-0.069	-0.269	1.510
	Analytical	1.237	0.830	0.630	1.510
1	FEM	4.213	-0.266	-3.946	10.502
	Analytical	5.280	0.800	-2.880	10.502
2	FEM	62.610	-0.906	-1.706	120.911
	Analytical	64.200	0.680	-60.120	120.911
4	FEM	982.600	-1.066	-981.500	1753.53
	Analytical	983.800	0.200	-980.200	1753.53

6	FEM	4956	7.199	-4963.6	8709.10
	Analytical	4948	-0.600	-4971.4	8709.10

It can be seen from Table 8 that the normal stresses obtained analytically and by FEM do not agree in most cases. However, the von Mises stress values in all cases agree very well. This test shows that even at very high deformation states which result in both geometric and material nonlinearities, von Mises stress can be uniquely and accurately determined under Dirichlet boundary conditions. The deformation states for different values of α used in this test are shown in Figure 10.

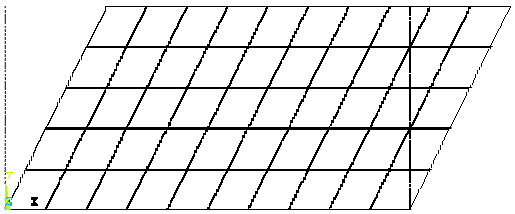

α = 0.5

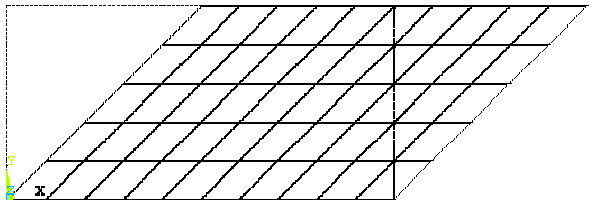

α = 1

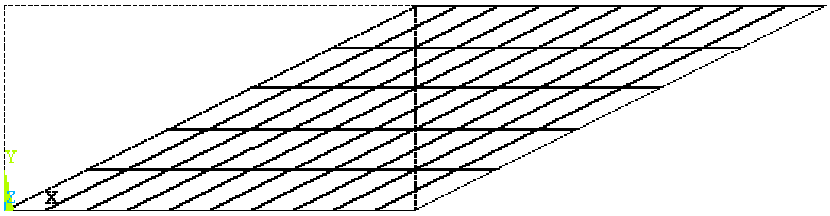

α = 2

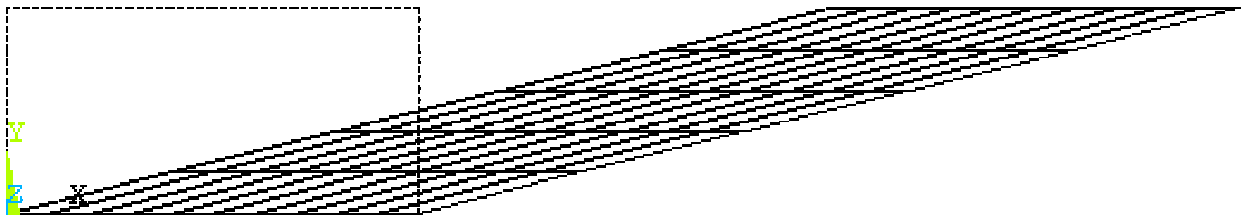

α = 4

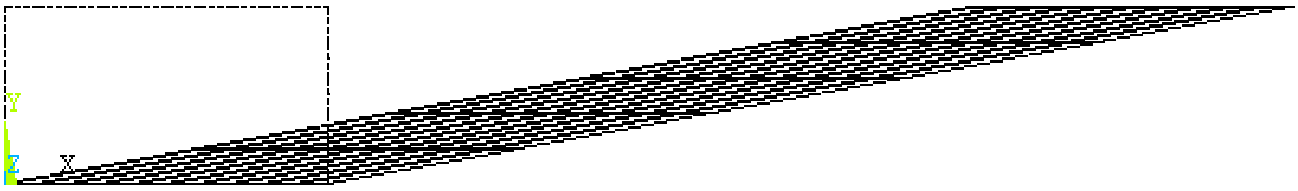

α = 6

Figure 10: Large Deformation States for a Plate in Simple Shear

4.1.2.1 Error Analysis

Similar to the error analysis discussed in section 4.1.1.1, an error analysis with constant and random errors for nonlinear analysis is performed to determine the performance of the hypothesis under nonlinear (material and geometric) circumstances.

4.1.2.1.1 Constant Error in Boundary Displacements

The deformation state α = 0.5 shown in Figure 10 is chosen for analysis.

Analytical Solution: σ_{eqv} = 1.51 kPa

Table 9: Error in von Mises stress due to constant displacement error

%Error in boundary displacements	σ_{eqv} [kPa]	% Error
1	1.545	2.357
2	1.581	4.761
3	1.618	7.210
4	1.656	9.706

4.1.2.1.2 Random Error in Boundary Displacements

For this part of the study, initially deformation states corresponding to $\alpha = 2$ and later $\alpha = 1$ deformation states were chosen. At higher values of random errors, however, problems with solution convergence were encountered. The prescribed displacements must be compatible with the incompressibility condition (no volume change). It was noted that this condition is significantly violated for large deformation states with error in boundary displacements. Thus, the finite element formulation fails. Ten different sets of random errors were chosen for each error level and the corresponding maximum errors in von Mises stress are reported below for the deformation state $\alpha = 0.5$.

Analytical Solution: σ_{eqv} = 1.510 kPa (for displacements without error)

Table 10: Maximum displacement error of 1%

Random Set No	Maximum σ_{eqv} [kPa]	% Error in Maximum σ_{eqv}
1	1.731	14.686
2	1.725	14.292
3	1.896	25.586
4	1.711	13.352
5	1.745	15.621
6	1.825	20.902
7	1.616	7.0317
8	1.888	25.034
9	1.748	15.821
10	1.682	11.390

Table 11: Maximum displacement error of 2%

Random Set No	Maximum σ_{eqv} [kPa]	% Error in Maximum σ_{eqv}
1	1.939	28.421
2	1.827	21.006
3	1.918	27.060
4	1.745	15.624
5	1.819	20.525
6	2.014	33.387
7	1.860	23.191
8	2.099	39.004
9	2.017	33.635
10	1.972	30.596

Table 12: Maximum displacement error of 3 %

Random Set No	Maximum σ_{eqv} [kPa]	% Error in Maximum σ_{eqv}
1	2.347	55.460
2	2.317	53.451
3	2.280	50.991
4	2.288	51.552
5	2.417	60.116
6	2.250	49.030
7	2.268	50.257
8	2.140	41.724
9	2.385	58.004
10	2.343	55.165

Table 13: Maximum displacement error of 4 %

Random Set No	Maximum $\boldsymbol{\sigma_{eqv}}$ [kPa]	% Error in Maximum $\boldsymbol{\sigma_{eqv}}$
1	2.518	66.812
2	1.932	27.945
3	2.528	67.419
4	2.448	62.135
5	2.381	57.740
6	2.173	43.934
7	2.324	53.967
8	2.240	48.368
9	2.156	42.824
10	2.223	47.218

It is evident from the above results that the error in von Mises stress is very high even for small values of error in the boundary displacements for both constant and random error cases. Hence, it can be concluded that for nonlinear problems very accurate displacement values may be required in order to obtain von Mises stress within a reasonable accuracy.

4.1.3 Quasi - Dirichlet Patch Test

In this section, the quasi-Dirichlet patch test discussed in Section 3.5 is performed on the Q4P1 element. Five arbitrary patches of elements shown in Figure 11 were chosen and the boundary displacements that correspond to a uniform von Mises stress field are prescribed. In such a scenario it is expected that the selected arbitrary patches of Q4P1 elements represent a uniform von Mises stress field. Arbitrary patches of elements were generated using a factor defined as the degree of distortion, D, and the von Mises stress was determined for different values of D. Degree of distortion, D, is defined as the percentage distortion of the common node of a patch of 4 elements in x and y directions with respect to its initial position as shown in Figure 11.

Example: If a and b are the element edge lengths in the x and y directions, respectively and D = 10%, then the centre node is moved by $\left(\frac{10}{100}\times a\right)$ in the x-direction and $\left(\frac{10}{100}\times b\right)$ in the y-direction.

It was noted that all the 5 arbitrary patches of elements resulted in uniform von Mises stress fields and are as tabulated in Table 14.

Table 14: Degree of distortion versus von Mises stress (α = 0.5)

Degree of Distortion (D)	σ_{eqv} [kPa]
0%	1.51004
10%	1.51004
20%	1.51004
30%	1.51004
40%	1.51004
45%	1.51004

Thus, it can be concluded that the element Q4P1 passes the quasi-Dirichlet patch test and hence convergence of the von Mises stress is possible. Deformed finite element grids for different values of D are shown in Figure 11.

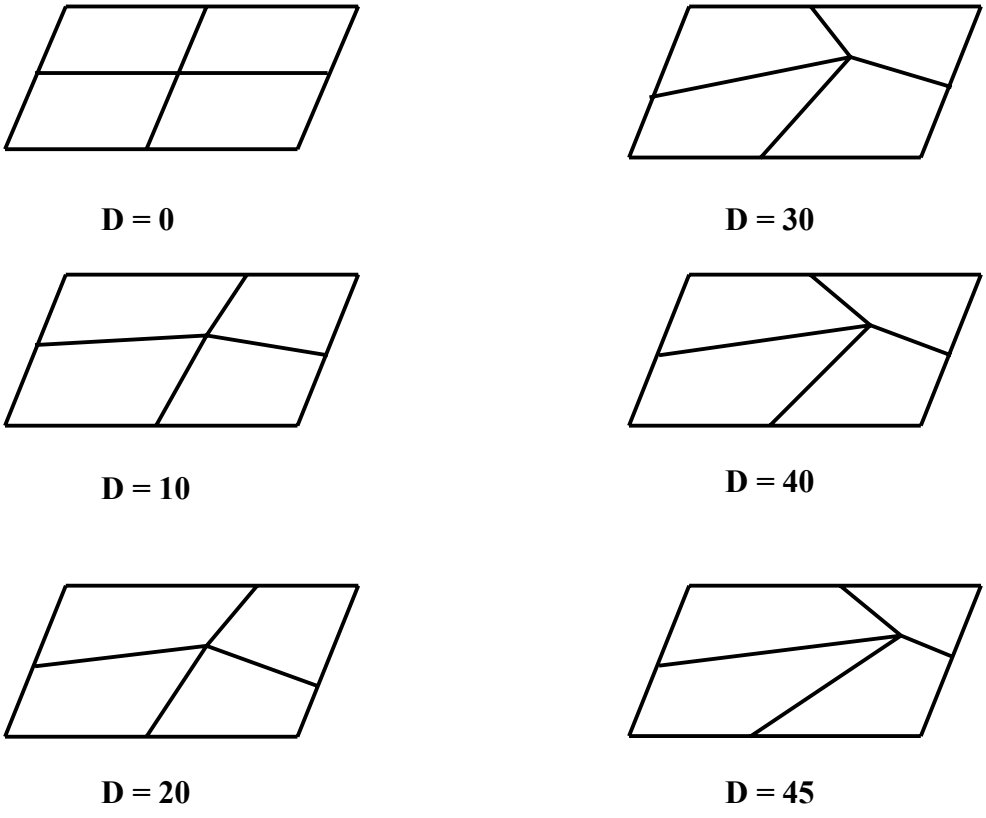

Figure 11: Arbitrary Patches of Q4P1 Elements

4.1.3.1 Count Condition Test

In this section, the effect of the count condition discussed in Section 2.5 on the resulting von Mises stress is studied. Different values of the count condition, and the corresponding von Mises stress values are reported in Table 15.

Table 15: Count condition versus von Mises stress

Mesh Size	N_u	N_p	$C = N_u / N_p$	Count Condition	von Mises Stress [kPa]
1 × 1	0	1	0	Violated	1.51004
2 × 1	0	2	0	Violated	1.51004
2 × 2	2	4	0.5	Violated	1.51004
3 × 2	4	6	0.67	Violated	1.51004
4 × 4	18	16	1.125	Satisfied	1.51004
6 × 6	50	36	1.388	Satisfied	1.51004
15 × 15	392	225	1.742	Satisfied	1.51004
100 × 100	19602	10000	1.9602	Satisfied	1.51004

From Table 15 it is evident that violation of the count condition does not affect the resulting von Mises stress. Therefore, it can be concluded that although the Q4P1 element does not satisfy the actual patch test, it satisfies the quasi Dirichlet patch test and thus, the convergence of normal stress differences, the shear stress values and hence the von Mises stress can potentially be achieved when this element is used for a Dirichlet problem.

4.2 Expansion of a Thick Walled Cylinder

In this section, expansion of a thick walled cylinder [28], as shown in Figure 12, is considered to investigate the hypothesis. For simulation purposes, only a 90 degree sector of the cylinder is considered, taking advantage of symmetry and symmetric boundary conditions. The geometry and boundary conditions of the original problem are shown in Figure 12. The problem shown in Figure 12 is in fact posed as a displacement problem by prescribing the nodal displacements in the global x and y directions as shown in Figure 13, and the von Mises stress is evaluated. The problem is solved in Cartesian coordinates and then the results are transformed into cylindrical coordinates in ANSYS®. For analysis, the continuum is discretized into a finite element grid of 20 × 10 elements. The Mooney-Rivlin coefficients used to simulate the hyperelastic behaviour are obtained from [28] as C_1 = 80 psi and C_2 = 20 psi.

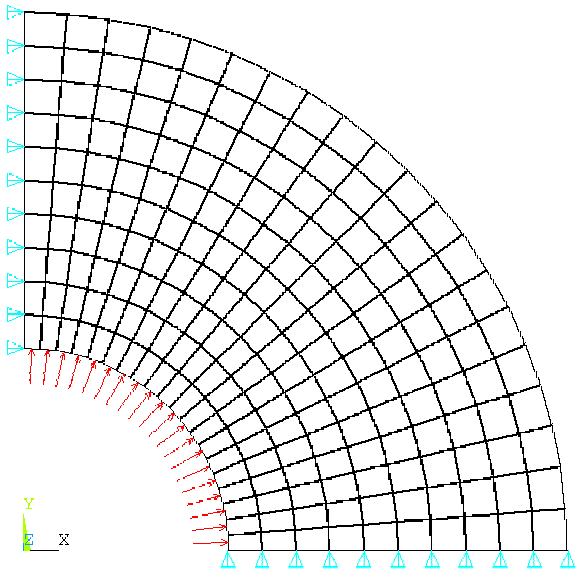

Figure 12: FEM Model of a Thick Walled Cylinder

4.2.1 Linear Analysis

A small deformation, linear stress-strain behaviour is considered in this section. The Young's modulus of the material is calculated as,

$$E = 6(C_1+C_2) = 6(80+20) = 600 \text{ psi}$$

Analysis details:

Element type: Plane 42 (4 node quadrilateral - displacement formulation) in plane strain.

Dimensions: Outer radius = 18.625 in. and inner radius = 7 in.

Finite element mesh: 20 × 10 elements.

Material type: Linear elastic

Analysis type: small deformation (Pressure = 10 psi).

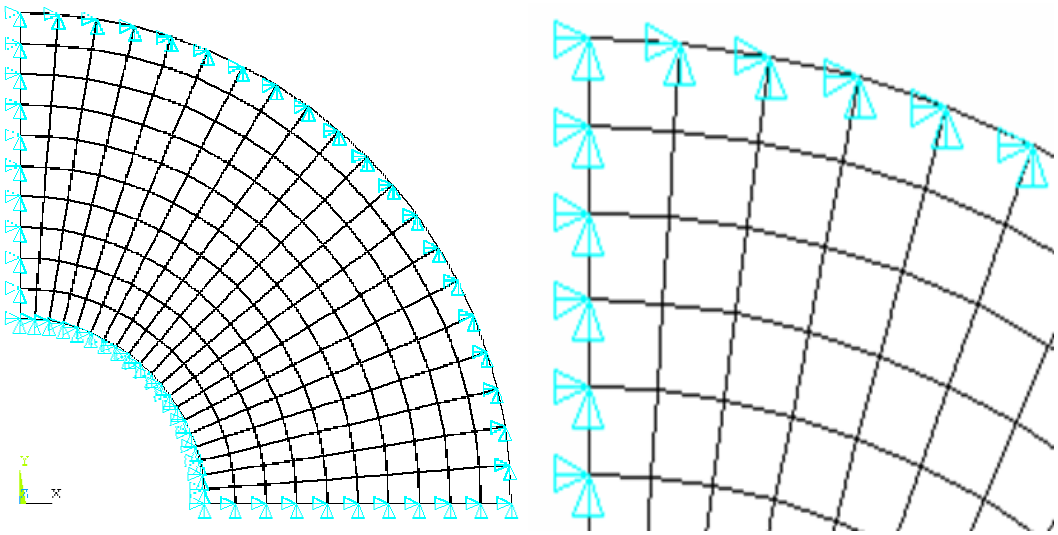

Figure 13: Dirichlet problem (Left), magnified view (right)

The Poisson's ratio of the material is varied from $0.49_{[1]}$ to $0.49_{[6]}$ and the results are tabulated in Table 16. The analytical solution for this case is obtained from [30] as,

$\sigma_r = 10$ psi, $\sigma_\theta = 13.289$ psi, $\sigma_z = 0$ and $\sigma_{eqv} = 20.236$ psi

Table 16: Finite element solution – Poisson's ratio Vs von Mises stress

Poisson's ratio	σ_r [psi]	σ_θ [psi]	σ_z [psi]	σ_{eqv} [psi]
$0.49_{[1]}$	-9.0499	14.888	2.8606	20.731
$0.49_{[2]}$	2.5419	26.385	14.435	20.649
$0.49_{[3]}$	117.84	141.67	129.73	20.637
$0.49_{[6]}$	0.1×10^6	0.1×10^6	0.1×10^6	20.634

The results presented in Table 16 show that when displacement based FEM is used for linear elastic incompressible materials, although the normal stresses are incorrect it is still possible to obtain unique and stable von Mises stress values within an accuracy of 2.5 %.

4.2.1.1 Error Analysis:

For the purposes of error analysis, a random displacement error case with maximum error of 2% is selected and error in the von Mises stress is evaluated. Table 17 shows the results.

Table 17: Effect of Random Error in Displacements on von Mises Stress

Random error	Maximum σ_{eqv} [kPa]	% Error in Maximum σ_{eqv}
Max value = 2%	21.021	3.87

From Table 17, it is evident that the error in von Mises stress is about 3.87% for a maximum 2% error in the prescribed boundary displacements. Thus, for this linear analysis, the solution error is of the same order of magnitude of the data error.

4.2.2 Nonlinear Analysis

In this section, the problem shown in Figure 13 is modeled using nonlinear Mooney – Rivlin hyperelastic material. The mixed u-p formulation Q4P1 element is used to generate the finite element model. In Table 18, normal and von Mises stress values at the inner radius of the cylinder for different deformation states are reported.

Analysis Details:

- **Dimensions:** Outer radius = 18.625 in and inner radius = 7 in.
- **Finite element mesh:** 20 × 10 elements.
- **Boundary conditions:** Displacements 'u' and 'v' along the boundary are prescribed.
- **Material:** Mooney – Rivlin hyperelastic material model, Poisson's Ratio = 0.49
- **Element type:** Hyper56 (Q4P1) – Mixed u-p formulation in plane strain.

Table 18: Stress states for various deformation states

Pressure Psi	Data type	σ_r [psi]	σ_θ [psi]	σ_z [psi]	σ_{eqv} [psi]
25	Pressure data	-22.144	34.633	2.980	49.279
	Displacement data	-26.9175	29.969	-1.653	49.367
50	Pressure data	-44.419	77.279	6.763	105.837
	Displacement data	-55.547	66.335	-4.076	105.977
100	Pressure data	-89.397	210.579	20.850	262.809
	Displacement Data	-122.192	177.599	-11.297	262.540
125	Pressure data	-112.157	331.422	36.509	391.049
	Displacement data	-165.313	276.350	-15.890	389.100

150	Pressure data	-135.221	555.570	69.883	614.473
	Displacement data	-225.443	453.798	-20.444	603.448

It is evident from Table 18 that the normal stress values obtained from pressure and displacement data do not agree in most of the cases, but the von Mises stress lies within a maximum deviation of 1.6%. Various deformation states which indicate the amount of geometric nonlinearity involved in the above analyzes are shown in Figure 14.

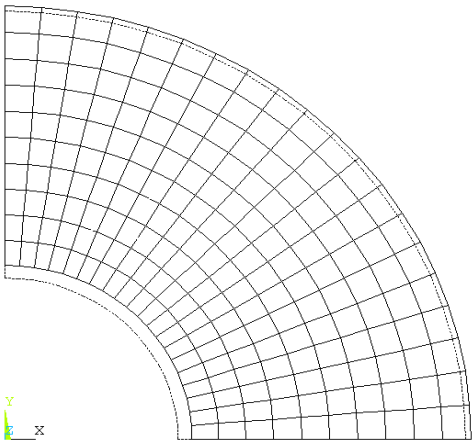

Internal Pressure = 25 psi

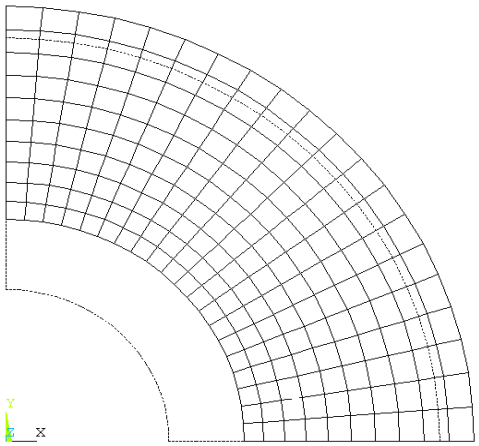

Internal pressure = 100 psi

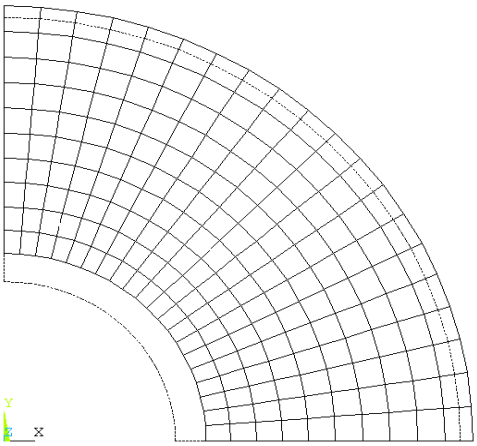

Internal Pressure = 50 psi

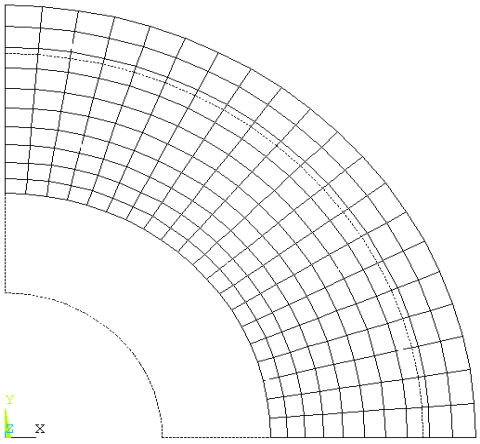

Internal pressure = 125 psi

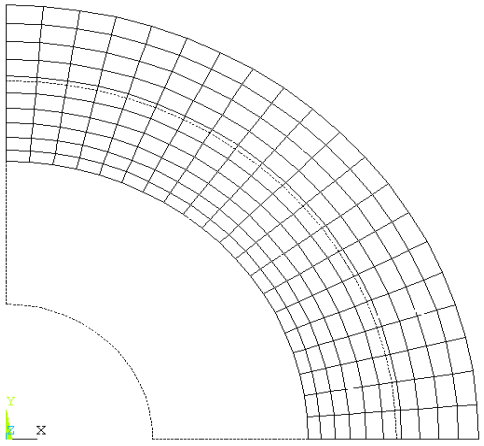

Internal pressure = 150 psi

Figure 14: Deformation of a Thick Walled Cylinder for Different Internal Pressure values

4.2.2.1 Error Analysis

In this section, a random displacement error case with the maximum error being 2% is considered and the error in von Mises stresses is evaluated.

Table 19: Effect of random error in displacements on von Mises stress

Random error	Maximum σ_{eqv} [psi]	% Error in Maximum σ_{eqv}
Max value = 2% (For 100psi)	265.6432	1.07

From Table 19, it is apparent that the error in the von Mises stress is of the same order of the error in the displacement data. Recall, however, the results for the simple shear problem in Section 4.1 showed significant error magnification when random errors were added to the boundary displacements. Therefore, the effect of error in displacements

depends on the nature of the problem and the class of deformation. Hence, it is not possible to draw a general all encompassing conclusion on the percentage error in the von Mises stress due to error in the boundary displacements.

4.2.3 Convergence of von Mises Stress

From the discussion in Section 4.1.3, the Q4P1 element when used to solve the Dirichlet problem of the incompressible case can result in convergence of the von Mises stress as the finite element grid is refined. In this section the actual convergence of von Mises stress is demonstrated. Figure 15 shows the convergence plot of the finite element solution (internal pressure = 100 psi) for the von Mises stress at the inner radius of the cylinder.

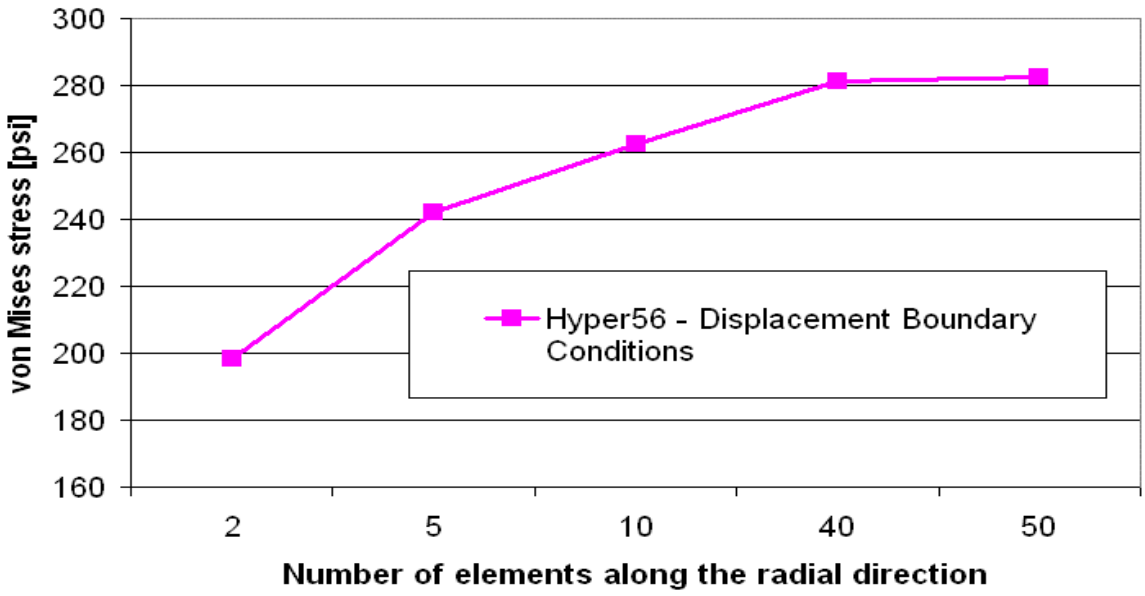

Figure 15: Convergence of von Mises stress

From Figure 15 it is evident that the von Mises stress value approaches a unique value as the number of elements in the finite element grid is increased. This implies that the von Mises stress approaches the exact value with the refinement of the finite element grid when the Q4P1 element is used to solve the Dirichlet problem.

4.3 A Plate in Uniform Strain

The next problem considered for study is a plate in uniform plane strain. The analytical solution for the linear elastic case is given by equation (51). For nonlinear analysis, the problem solved using ANSYS® with force boundary conditions is used as a reference for comparison. The original problem is as shown in Figure 16(a), which is a plate of dimensions b × h subjected to pressure, P, resulting in a uniform stress/strain field. This problem is posed as a Dirichlet problem as shown in figure 16 (b) and the hypothesis is tested for linear elastic and hyperelastic cases.

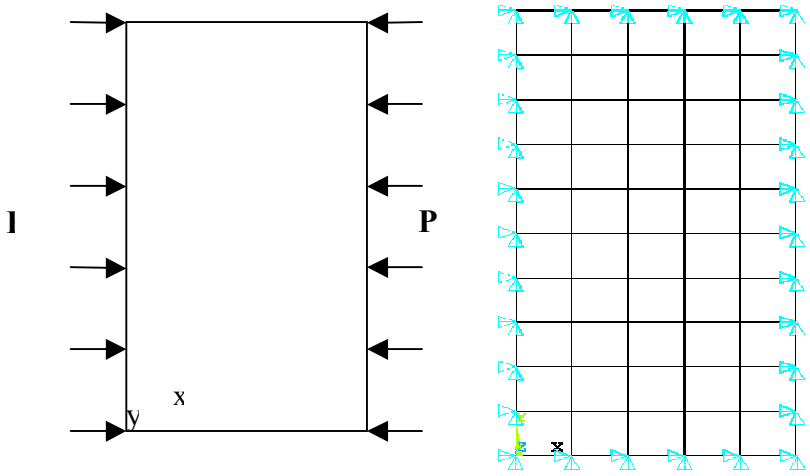

(a) (b)

Figure 16: Plate in uniform strain- (a) Original problem (b) Finite element model

4.3.1 Linear Elastic Analysis

When a plate is subjected to pressure, P, as shown in Figure 16, the displacement fields u, and, v, in the x and y directions respectively can be written as,

$$u = -P\frac{(1-\nu^2)}{E}\left(x-\frac{b}{2}\right), \qquad v = P\nu\frac{(1+\nu)}{E}\left(y-\frac{h}{2}\right) \tag{51}$$

where

P = 100 MPa , ν = 0.5, E = 70,000 MPa, b = 100 mm and h = 200 mm.

Analysis details:

- Plate: 100 mm × 200 mm
- **Boundary conditions:** Dirichlet boundary conditions
- **Material:** Linear elastic material model.
- **Element type:** Plane42. [4 node quadrilateral element – displacement]
- **Analysis type:** Plane strain, small deformation, linear elastic analysis

Analytical solution (for $\nu = 0.4999$)**:** $\sigma_X = 100$ MPa, $\sigma_Y = 0$, $\sigma_Z = 50$ MPa,

$$\sigma_{eqv} = 86.603 \text{ MPa.}$$

Table 19: Linear elastic solution – Poisson's ratio Vs stress state

Poisson's ratio	σ_x [MPa]	σ_y [MPa]	σ_z [MPa]	σ_{eqv} [MPa]
0.45	-51.734	51.713	-0.931E-02	89.588
0.49	-50.386	50.285	-0.493E-01	87.183
0.49[2]	-50.533	49.533	-0.499E	86.660
0.49[3]	-55.004	45.002	05	86.608
0.49[5]	-550.033	-450.03	-500.03	86.602
0.49[8]	-500083	-499983	-500033	86.608

The results presented in Table 19 indicate that even when $\nu = 0.49$[8] it is still possible to obtain the von Mises stress with in an acceptable accuracy. This confirms that the use of displacement based FEM for linear elastic incompressible materials can result in an accurate von Mises stress value up to a certain limit of ν.

4.3.2 Nonlinear Analysis

Similar to the nonlinear analyzes in the previous examples, the plate is modeled as a nonlinear hyperelastic Mooney – Rivlin material. Large deformation analysis of the Dirichlet problem is performed. The results are compared with those obtained from solving the same problem using pressure boundary conditions as shown in Figure 16(a). The stress state is uniform over the entire body and is as presented in Table 20.

- **Plate :** 100 mm × 200 mm
- **Boundary conditions:** Displacements, u, and, v, along the boundary are prescribed.
- **Material:** Mooney – Rivlin hyperelastic material model, Poisson's Ratio = 0.49
- **Element type:** Hyper56 (Q4P1) – Mixed u-p formulation in plane strain.
- **Analysis type:** Large deformation - nonlinear analysis

Table 20: von Mises Stress at different deformation states

Pressure MPa	Data type	σ_x [MPa]	σ_y [MPa]	σ_z [MPa]	σ_{eqv} [MPa]
100	Pressure data	-99.999	-0.168E-03	-50.034	86.601
	Displacement data	-5051.14	-4951.140	-5001.17	86.602
500	Pressure data	-499.97	-0.1E-01	-282.35	434.186
	Displacement data	-26316.9	-25816.9	-26099.3	434.186

1000	Pressure data	-999.9040	-0.3294E-01	-639.418	877.070
	Displacement Data	-55098.632	-54098.761	-54738.14	877.070
1500	Pressure data	-1499.814	-0.6411E-01	-1044.577	1331.821
	Displacement data	-85466.875	-83967.125	-85011.63	1331.820

The deformed configurations for the values of pressure presented in Table 20 are shown in Figure 17,

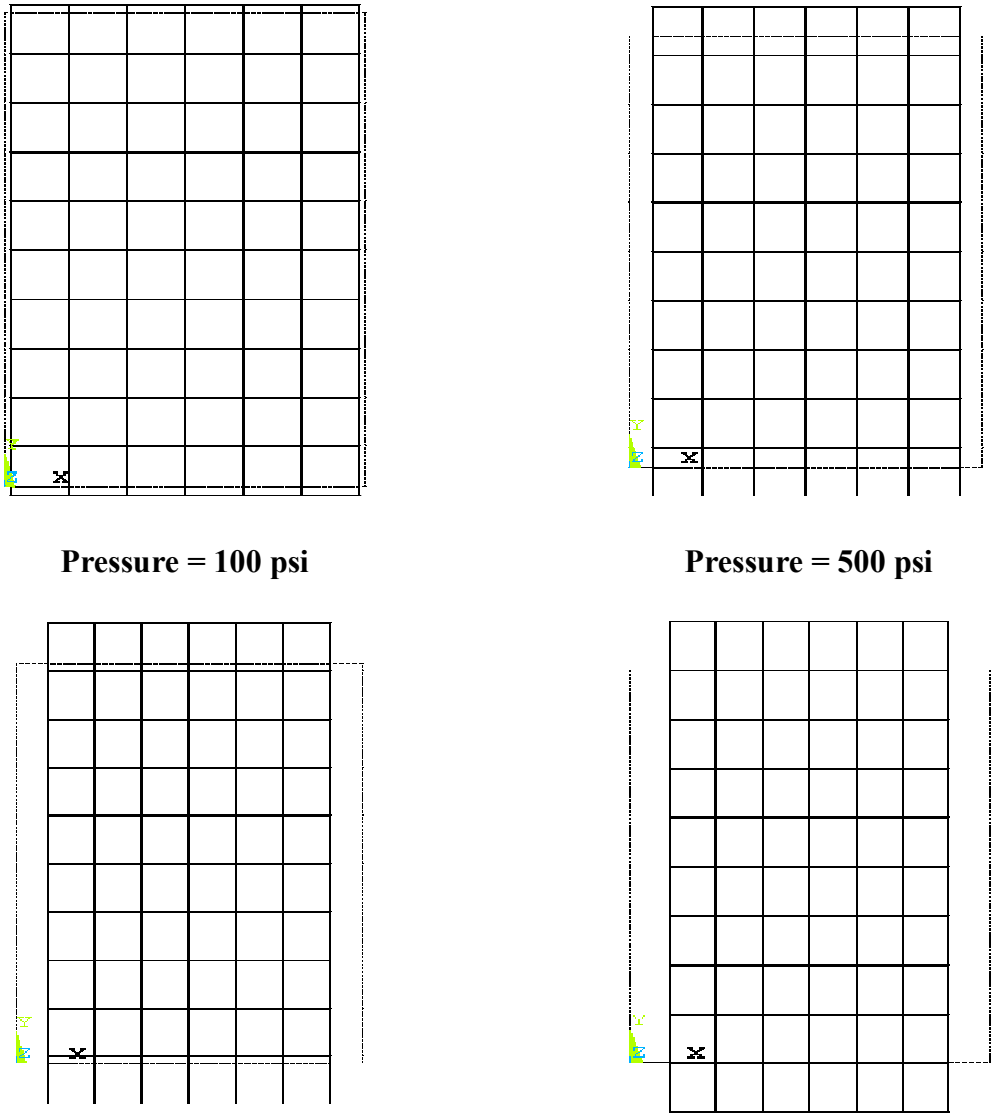

Pressure = 100 psi **Pressure = 500 psi**

Pressure = 10000 psi **Pressure = 15000 psi**

Figure 17: Plate in uniform strain – different deformation states

4.4 Cook's Membrane

Cook's membrane is one of the most widely used problems in the literature to test finite element formulations and concepts in solid mechanics. Here, the Cook's membrane is used as a last numerical example to verify the hypothesis presented in Chapter 3. The geometry, boundary and loading conditions of Cook's membrane as used in the literature and the corresponding Dirichlet problem used in the current work are shown in Figure 18. In similar fashion to the previous examples, a numerical analysis of linear and nonlinear cases is considered. An analytical solution to this problem is not available due to the complexity of the geometry and deformation. Hence, the solution obtained by solving the problem using force boundary conditions is used as a reference.

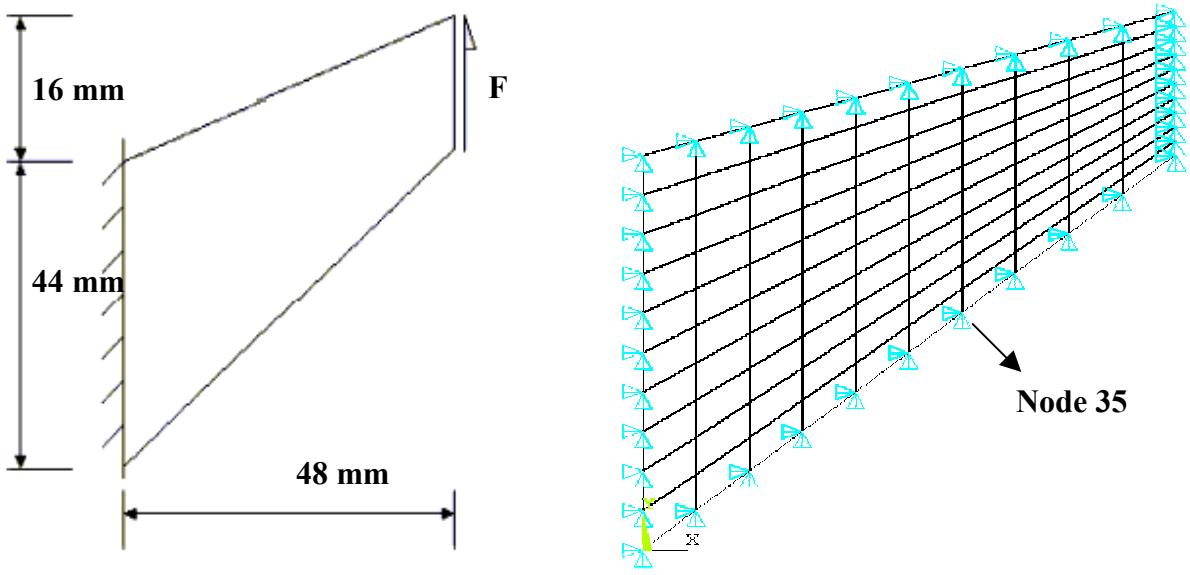

Figure 18: Cook's Membrane – Original and the Dirichlet problems

4.4.1 Linear Elastic Analysis

In linear elastic analysis, the problem is modeled using the 4 node quadrilateral – displacement based elements. Normal stress and von Mises stress values obtained for various values of Poisson's ratio are tabulated in Table 21. The stress field is non-uniform over the entire membrane and hence, the stresses at only one node (node 35, Figure 18) are presented. For this problem, the stress values obtained using pressure boundary conditions along with the finite element Hyper56 are used for comparison.

Analysis details:

- **Boundary conditions:** Dirichlet boundary conditions,
- **Material:** Linear elastic material model, E = 2040 MPa,
- **Element type:** Plane42. [4 node quadrilateral element – displacement],
- **Analysis type:** Plane strain, small deformation, linear elastic analysis.

A very small deformation state is chosen i.e. F = 0.5 kN. The solution obtained from force boundary conditions for $\nu = 0.49$ is, σ_x = 58503 MPa, σ_y = 54416 MPa, σ_z = 50691 MPa and σ_{eqv} = 97040 MPa.

Table 21: Poisson's ratio vs stress state

Poisson's ratio	$\boldsymbol{\sigma_x}$ MPa	$\boldsymbol{\sigma_y}$ MPa	$\boldsymbol{\sigma_z}$ MPa	$\boldsymbol{\sigma_{eqv}}$ MPa
0.45	35091	5437.5	18238	100880
0.49	-90222	-134290	-110010	108130
$0.49_{[2]}$	-1614E03	1663 E03	-1635 E03	110640
$0.49_{[3]}$	-16887E03	16937 E03	-16908 E03	110830
$0.49_{[5]}$	-0.16969E10	-0.16970 E10	-0.16969 E10	110890

From the results presented in Table 21, it can be seen that although the normal stresses are highly inaccurate, the normal stress differences and shear stress values agree well with the reference values for the von Mises stress. It is important to note that the results used for comparison were obtained using the finite element method and therefore the reference solution is approximate itself. However, it can be noted that as the value of Poisson's ratio approaches one-half, the error in the von Mises stress increases. Therefore, when a linear elastic incompressible material is modeled as a Dirichlet problem using the displacement based finite elements and analyzed for von Mises stress, it is advisable to take care in selecting the value of Poisson's ratio.

4.4.2 Nonlinear Analysis

In this section, both material and geometric nonlinearities of the problem are considered. Here, the results for stresses obtained by solving the Dirichlet problem for four different deformation states presented in Figure 19 are presented.

- **Boundary conditions:** Displacements u and v along the boundary are prescribed.
- **Material:** Mooney – Rivlin hyperelastic material model, Poisson's Ratio = 0.4999
- **Element type:** Hyper56 (Q4P1) – Mixed u-p formulation in plane strain.
- **Analysis type:** Large deformation - nonlinear analysis

Table 22: von Mises Stress at different deformation states

Force [kN]	Data type	σ_x [MPa]	σ_y [Mpa]	σ_z [MPa]	σ_{eqv} [MPa]
1.61	Force data	100.64	231.15	138.23	282.10
	Displacement data	2777.20	2843.10	2776.80	292.98
3.23	Force data	212.42	447.67	231.43	562.33
	Displacement data	5729.50	5975.80	5754.30	560.62
6.47	Force data	261.22	921.53	327.06	1013.60
	Displacement Data	11575.00	12266.00	11653.00	1039.00
9.7	Force data	269.12	1350.10	373.47	1398.00
	Displacement data	17270.00	18414.00	17391.00	1458.90

Table 22 shows that the von Mises stress values obtained from pressure and displacement boundary conditions are within a deviation of 4.35%, whereas the normal stress values are not comparable. Hence, the hypothesis discussed in Section 3.5 is validated.

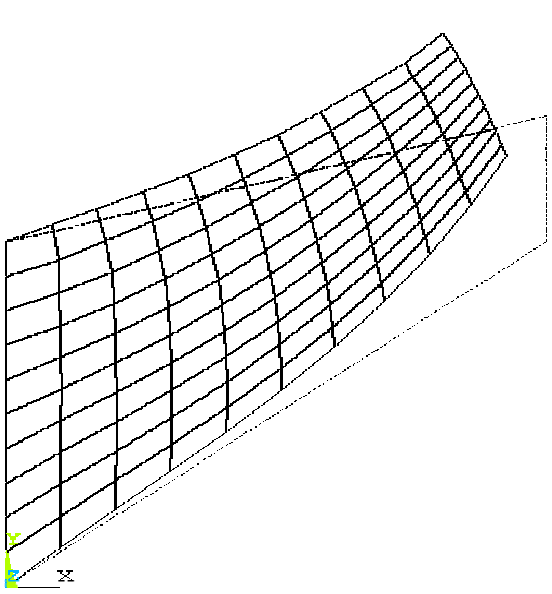

F = 1.61 kN

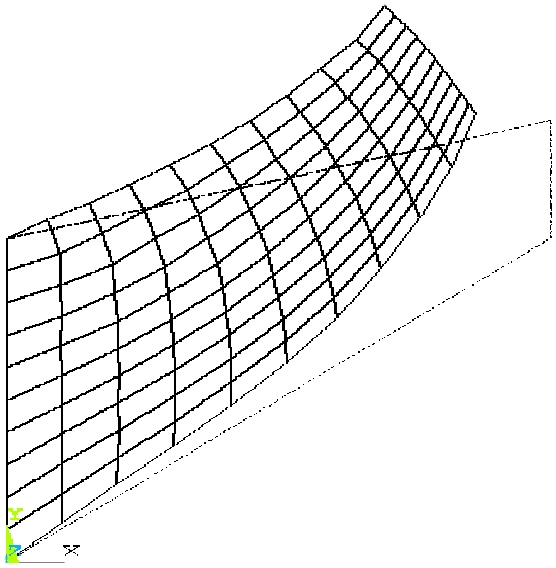

F = 3.23 kN

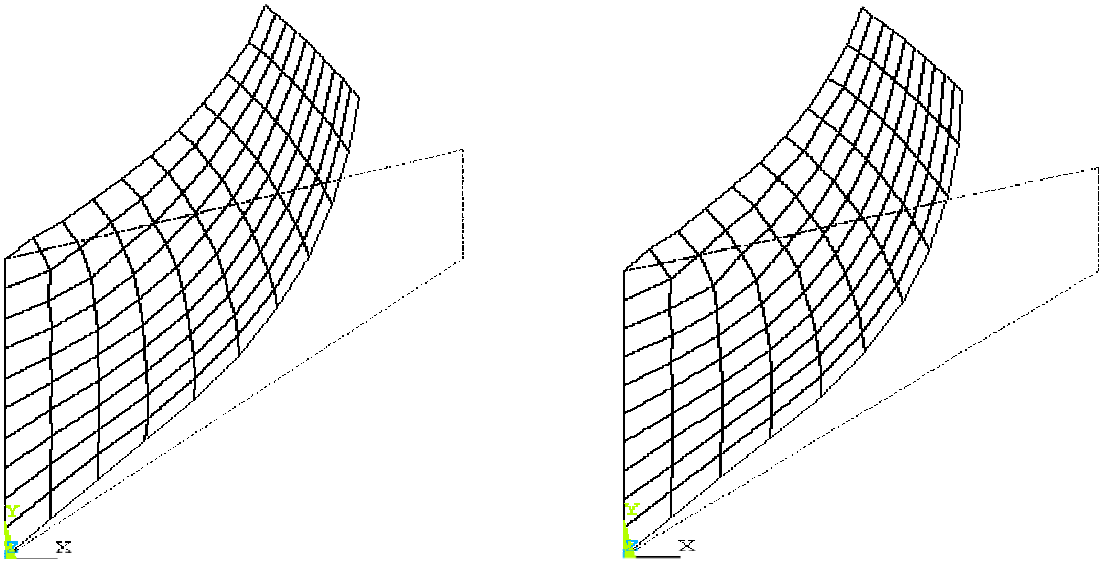

F = 6.47 kN **F = 9.7 kN**

Figure 19: Cook's membrane – Nonlinear deformation

Chapter 5

Summary and Conclusions

5.0 Introduction

This chapter briefly summarizes the research work discussed in this thesis. Conclusions are drawn based on the numerical results presented in Chapter 4.

5.1 Summary

It is often important to determine the material properties of soft tissues such as skin for better understanding of their physiological behaviour. One method of realizing this is by using high resolution images of soft tissues in various deformed and undeformed configurations, from which the displacement data can be obtained. The displacement data obtained in this way can be used in conjunction with the conventional finite element method in the inverse mode to obtain the material properties. Finite element analysis of soft tissues is not straightforward due to the fact that they are incompressible in nature. When displacements along the boundary are prescribed for an incompressible material and an attempt is made to calculate the stress field within the body, the system of equations used to solve for the unknowns become highly ill-conditioned and hence unstable. In the current work, finite element analysis of the incompressible case under Dirichlet boundary conditions is considered. It has been hypothesized that, although it is not possible to obtain the entire stress state due to non-uniqueness of hydrostatic pressure,

there is enough information to reliably calculate the normal stress differences, shear stresses and hence the von Mises stress. The main objective of this research project has been to numerically investigate this hypothesis. The effectiveness of the hypothesis is tested with the aid of four numerical examples which deal with different deformation scenarios.

5.2 Conclusions

The following are the conclusions that are drawn based on the numerical results presented in Chapter 4.

For both linear and nonlinear problems with no data error (i.e. no simulated measurement error added to the boundary displacement data), the numerical results obtained in this research confirm the theoretical result that stable values of the von Mises stress can potentially be obtained from incorrect/unstable values of σ_X, σ_Y and σ_Z, together with the calculated values of the shear stresses.

It must be emphasized, however, that these results do not constitute a proof that the von Mises stress can always be obtained. In order to have confidence in the resulting von Mises stress where the data values are accurate, more tests, of greater complexity, and possibly additional theoretical investigations regarding the numerical possesses are required.

Similarly, the results for linear and nonlinear problems with uniform data error show promise, although again more testing would be required to permit any positive generalizations about the accuracy of von Mises stress.

For both linear and nonlinear problems with random data error, the results indicate that the calculated values of von Mises stress are unreliable and may be subject to significant error as compared to the error in the data. It is the author's observation, however, that the random errors in the boundary displacements result in a mathematical contradiction where the boundary displacements violate the constant volume nature of the incompressible material. It is the author's speculation that the error magnification may be primarily due to this inconsistency.

References

[1] Fried, I., "Influence of Poisson's Ratio on the Condition of the Finite Element Stiffness Matrix," International Journal of Solids and Structures, Vol. 9, PP. 323-329, 1973.

[2] Nagtegaal, J. C., Parks, D. M. and Rice, J. R., "On Numerically Accurate Finite Element Solutions in the Fully Plastic Range," Computer Methods in Applied Mechanics and Engineering, Vol. 4, PP. 153-174, 1974.

[3] Gadala., M. S., "Numerical Solutions of Nonlinear Problems of Continua—II. Survey of Incompressibility Constraints and Software Aspects," Computers & Structures, Vol. 22, PP. 841-855, 1986.

[4] Beatty, M.F., "Topics in finite elasticity: hyperelasticity of rubber, elastomers and biological tissues with examples," Applied Mechanics Review Vol. 40, PP. 1699–1734, 1987.

[5] ANSYS® user's manual – Analysis Guide (on-line), Version 9.0, ANSYS Inc., 2005

[6] Zienkiewicz., O. C., Qu, S., Taylor, R. L., Nakazawa, S., "The patch test for mixed formulations," International Journal of Numerical Methods in Engineering, Vol. 23, PP.1873–83, 1986.

[7] Ernest, D., George, Jr., George, A. H. and Stephen, J., "The integration of analysis and testing for the simulation of the response of hyperelastic materials," Finite Elements in Analysis and Design, Vol. 4, PP. 19-42, 1988.

[8] Bonet, J., Wood, R. D., Nonlinear continuum mechanics for nonlinear analysis, Cambridge University Press, 1997.

[9] Mooney, M., "A Theory of Large Elastic Deformation," Journal of Applied Physics, Vol.11, 582—592, 1940.

[10] Rivlin, R. S., "Large elastic deformation of isotropic materials," Philosophical Transactions of the Royal Society of London, Vol. A 195, PP 463-473, 1949.

[11] Bathe, K.J, 1996, Finite Element Procedures, Prentice Hall.

[12] Cook, R.D., Malkus, D.S., Plesha, M.E., Witt, R.J., 2001, Concepts and applications of Finite Element Analysis., 4th Ed., John Wiley and sons. Inc.

[13] Fung, Y.C., Tong, P., Classical and Computational Solid Mechanics, World Scientific, 2001.

[14] Zienkiewicz, O.C.; Taylor, R.L., Finite Element Method (5th Edition) Volume 1 - The Basis, Elsevier, 2000.

[15] Herrmann., L. R., "Elasticity equations for nearly incompressible materials by a variational theorem," AIAA Journal, 3, 1896–1900, 1965.

[16] Zienkiewicz., O. C., Holister., G. S., "Displacement and equilibrium models in the finite element method," by B. Fraeijs de Veubeke, Chapter 9, Pages 145–197 of Stress Analysis, International Journal of Numerical Methods in Engineering , Vol. 52, PP. 287–342, 2001.

[17] Scharnorst., T., Pian., T. H. H., "Finite element analysis of rubber like materials by a mixed model," International Journal of Numerical Methods in Engineering, Vol. 2, PP. 655–676, 1978.

[18] Key., S.W., “A variational principle for incompressible and nearly-incompressible anisotropic elasticity, International Journal of Solids and Structures,” Vol. 5, PP.951-964, 1969.

[19] Washizu., K., Variational Methods in Elasticity and Plasticity (Pergamon, Oxford, 1974).

[20] Jasbir .S. A., Introduction to Optimum Design, Mc Graw Hill, 1989.

[21] Taylor, R.L., Simo, J.C., Zienkiewicz, O.C., Chan, A.C.H., "THE PATCH TEST - A CONDITION FOR ASSESSING FEM CONVERGENCE." International Journal for Numerical Methods in Engineering Vol.22, PP. 39 - 62, 1986.

[22] Zienkiewicz, O.C.; Taylor, R.L., “The finite element patch test revisited: A computer test for convergence, validation and error estimates,” Computer Methods Appl. Mech. Engrg. 149 (1997) 223-254.

[23] Hughes, T.J.R., The Finite Element Method – Linear static and Dynamic Finite Element Analysis, Prentice-Hall Inc, 1987.

[24] Beer, P. F., Johnston, E.R., Mechanics of Materials, McGraw-Hill Ryerson Limited, 1985.

[25] Coley, L.M., Dolovich, A.T., Finite Element Calculations for Perfectly Incompressible Materials and Displacements Prescribed on the Entire Boundary, Submitted to CSME Transactions, February 2006.

[26] Ogden, R. W., Fu, Y.B., Nonlinear elasticity: theory and applications**,** Cambridge University Press, 2001.

[27] Coley, L., A finite element analysis of the Limberg flap used in plastic surgery, Master of Science thesis, University of Saskatchewan.

[28] Batra, R.C., "Finite plane strain deformations of rubberlike materials," International Journal for Numerical Methods in Engineering, 20-10, PP.145-156, 1980.

[29] Rao, D.V., Yuasa, T., Akatsuka, T., Tromba, G., Hasan, M.Z., Takeda, T., Devaraj, B., "Images of biological soft tissue using synchrotron X-ray and laser CT systems," Radiation Measurements, Vol. 41,177 – 182, 2006.

[30] Budynas, R.G., Advanced strength and applied stress analysis, WCB/McGraw-Hill, 1999

Appendix A

In this Appendix, the analytical solution for the "Simple Shear" problem considered in Section 4.1 is presented. The analytical solution was obtained using the MathCAD 2000 and is as shown below.

All Stresses are in Pascals

Mapping

$\alpha := 0.05$

$x = X + \alpha Y$

$y = Y$

$z = Z$

Identity Matrix

$$I := \begin{pmatrix} 1 & 0 & 0 \\ 0 & 1 & 0 \\ 0 & 0 & 1 \end{pmatrix}$$

Deformation Gradient

$$F := \begin{pmatrix} 1 & \alpha & 0 \\ 0 & 1 & 0 \\ 0 & 0 & 1 \end{pmatrix}$$

$J := |F|$

$J = 1$

Cauchy Green Tensor

$C := F^{T} \cdot F$

$$C = \begin{pmatrix} 1 & 0.05 & 0 \\ 0.05 & 1.002 & 0 \\ 0 & 0 & 1 \end{pmatrix}$$

Green Strain Tensor

$$E := \frac{1}{2}\cdot\left(F^{T}\cdot F - I\right)$$

$$E = \begin{pmatrix} 0 & 0.025 & 0 \\ 0.025 & 1.25 \times 10^{-3} & 0 \\ 0 & 0 & 0 \end{pmatrix}$$

Invariants of C

$$I_1 := C_{1,1} + C_{2,2} + C_{3,3}$$

$$I_1 = 3.002$$

$$I_2 := C_{1,1}\cdot C_{2,2} + C_{2,2}\cdot C_{3,3} + C_{3,3}\cdot C_{1,1} - C_{1,2}\cdot C_{2,1} - C_{2,3}\cdot C_{3,2} - C_{3,1}\cdot C_{1,3}$$

$$I_2 = 3.002$$

$$I_3 := 1$$

Mooney-Rivlin Material Coefficients (Pascals)

$$a_1 := 260$$

$$a_2 := 80$$

$$a_3 := 3940$$

$$a_4 := -4060$$

$$a_5 := 1070$$

Strain energy potential

$$W\left(I_1, I_2, I_3, I_4, I_5\right) := a_1\cdot\left(I_1 - 3\right) + a_2\cdot\left(I_2 - 3\right) + a_3\cdot\left(I_1 - 3\right)^2 + a_4\cdot\left(I_1 - 3\right)\cdot\left(I_2 - 3\right) \ldots + a_5\cdot\left(I_2 - 3\right)^2$$

Second Piola Kirchoff Stress

$$DI1C22 = \frac{d}{dC_{22}}\left(I_1\right)$$

$$DI1C22 := 1$$

$$DI2C22 := C_{1,1} + C_{3,3}$$

$$DI2C22 = 2$$

$$DI1C11 := 1$$

$$DI2C11 := C_{2,2} + C_{3,3}$$

$$DI2C11 = 2.002$$

$$DWI1 := a_1 + 2 \cdot a_3 \cdot (I_1 - 3) + a_4 \cdot (I_2 - 3)$$

$$DWI1 = 269.55$$

$$DWI2 := a_2 + a_4 \cdot (I_1 - 3) + 2 \cdot a_5 \cdot (I_1 - 3)$$

$$DWI2 = 75.2$$

$$DWI3 := 0$$

$$DI1C12 := 0$$

$$DI2C12 := (-C)_{2,1}$$

$$DI2C12 = -0.05$$

$$DI1C33 := 1$$

$$DI2C33 := C_{1,1} + C_{2,2}$$

$$DI2C33 = 2.002$$

$$DI1C23 := 0$$

$$DI2C23 := -C_{3,2}$$

$$DI1C31 := 0$$

$$DI2C31 := -C_{1,3}$$

$$S_{1,1} := 2 \cdot (DWI1 \cdot DI1C11 + DWI2 \cdot DI2C11)$$

$$S_{1,1} = 840.276$$

$$S_{2,2} := 2 \cdot (DWI1 \cdot DI1C22 + DWI2 \cdot DI2C22)$$

$$S_{2,2} = 839.9$$

$$S_{3,3} := 2 \cdot (DWI1 \cdot DI1C33 + DWI2 \cdot DI2C33)$$

$$S_{3,3} = 840.276$$

$$S_{1,2} := 2 \cdot (DWI1 \cdot DI1C12 + DWI2 \cdot DI2C12)$$

$S_{1,2} = -7.52$

$S_{2,1} := S_{1,2}$

$S_{2,1} = -7.52$

$S_{2,3} := 2 \cdot (DWI1 \cdot DI1C23 + DWI2 \cdot DI2C23)$

$S_{2,3} = 0$

$S_{3,2} := S_{2,3}$

$S_{3,2} = 0$

$S_{3,1} := 2 \cdot (DWI1 \cdot DI1C31 + DWI2 \cdot DI2C31)$

$S_{3,1} = 0$

$S_{1,3} := S_{3,1}$

$S_{1,3} = 0$

Therefore,

$$S = \begin{pmatrix} 840.276 & -7.52 & 0 \\ -7.52 & 839.9 & 0 \\ 0 & 0 & 840.276 \end{pmatrix}$$

CAUCHY STRESS TENSOR

$\sigma := F \cdot J^{-1} \cdot S \cdot F^{T}$

$$\sigma = \begin{pmatrix} 841.62375 & 34.475 & 0 \\ 34.475 & 839.9 & 0 \\ 0 & 0 & 840.276 \end{pmatrix}$$

von Mises Stress

$$\sigma_{eqv} := \frac{1}{\sqrt{2}} \cdot \left[\left(\sigma_{1,1} - \sigma_{2,2}\right)^2 + \left(\sigma_{2,2} - \sigma_{3,3}\right)^2 + \left(\sigma_{3,3} - \sigma_{1,1}\right)^2 + 6 \cdot \left[\left(\sigma_{1,2}\right)^2 + \left(\sigma_{2,3}\right)^2 + \left(\sigma_{3,1}\right)^2 \right] \right]^{\frac{1}{2}}$$

$\sigma_{eqv} = 59.73$ Pa

Appendix B

Input files for ANSYS®

In this appendix, the input files to the finite element package ANSYS® for all the numerical examples discussed in chapter 4 are presented

1. A Plate in Simple Shear

Linear Elastic Analysis:

```
alpha=0.05
/prep7
ET,1,plane42
keyopt,1,3,2
EX,1,0.2040
NUXY,1,0.4999
k,1,
k,2,0.1
k,3,0.1,0.05
k,4,,0.05
l,1,2
l,2,3
l,3,4
l,4,1
lplo
al,1,2,3,4
aplo
LSEL,S,LINE,,1
LESIZE,ALL,,,10
LSEL,S,LINE,,3
LESIZE,ALL,,,10
LSEL,S,LINE,,2
LESIZE,ALL,,,5
LSEL,S,LINE,,4
LESIZE,ALL,,,5
allsel
amesh,1
/pnum,nodes,0
eplo
/solu
lsel,s,line,,1,4
nsll,s,1
d,all,uy
allsel
ANTYPE,STATIC
/FORMAT,,,20,14
lsel,s,line,,1,4
nsll,s,1
*get,numloop,NODE,0,count
*do,i,1,numloop
*get,nodeload,NODE,NN,NXTH
*get,Yloc,NODE,nodeload,loc,Y
DeX=1.01*alpha*Yloc
d,nodeload,ux,DeX
NN=nodeload
*enddo
allsel
solve
/post1
pldisp,2
nsll,,1,4
plnsol,s,eqv
prnsolms
```

Nonlinear Elastic Analysis:

```
alpha=6
/prep7
ET,1,hyper56
MP,NUXY,1,0.499
TB,MOONEY,1,5
TBDATA,1,260E-03    !kpa
TBDATA,2,80E-03
TBDATA,3,3940E-03
TBDATA,4,-4060E-03
TBDATA,5,1070E-03
k,1,
k,2,1
k,3,1,0.5
k,4,,0.5
l,1,2
l,2,3
l,3,4
l,4,1
lplo
al,1,2,3,4
aplo
LSEL,S,LINE,,1,4
LESIZE,ALL,,,10
allsel
amesh,1
/pnum,nodes,0
eplo
/solu
lsel,s,line,,1,4
nsll,s,1
d,all,uy
allsel
ANTYPE,STATIC
NLGEOM,1
NSUBST,10,100,5
LNSRCH,0
NEQIT,100
pred,off
/FORMAT,,,20,14
lsel,s,line,,1,4
nsll,s,1
*get,numloop,NODE,0,count
*do,i,1,numloop
*get,nodeload,NODE,NN,NXTH
*get,Yloc,NODE,nodeload,loc,Y
DeX=alpha*Yloc
d,nodeload,ux,DeX
NN=nodeload
*enddo
allsel
solve
/post1
pldisp,2
nsll,,1,4
plnsol,s,eqv
prnsolms
```

2. Expansion of a Thick Walled Cylinder

Linear Elastic Analysis:

```
b=3.0022          !Deformation coefficient due to an internal pressure of 10Psi [28]
C1=80
C2=20
Youngsmodulus=6*(C1+C2)
/prep7
csys,0
ET,1,Plane42
KEYOPT,1,3,2
```

```
EX,1,Youngsmodulus
MP,NUXY,1,0.49
CYL4, , ,7,0,18.625,90
/pnum,line,1
lplo
LSEL,S,LINE,,1
LESIZE,ALL,,,20
LSEL,S,LINE,,3
LESIZE,ALL,,,20
LSEL,S,LINE,,2
LESIZE,ALL,,,10
LSEL,S,LINE,,4
LESIZE,ALL,,,10
allsel
amesh,1
/solu
ANTYPE,STATIC
/FORMAT,,,20,5
lsel,s,line,,1,4
nsll,s,1
*get,numloop,NODE,0,count
*do,i,1,numloop
*get,nodeload,NODE,NN,NXTH
*get,Yloc,NODE,nodeload,loc,Y
*get,Xloc,NODE,nodeload,loc,X
        R=sqrt(Xloc**2+Yloc**2)
        costheta = Xloc/R
        sintheta = Yloc/R
        Ur=-R+sqrt(R**2+b)
        DeX= Ur*costheta
        DeY= Ur*sintheta
        d,nodeload,ux,DeX
        d,nodeload,uy,DeY
        NN=nodeload
*enddo
allsel
solve
/post1
rsys,1
nsel,s,,,42
prnsolms
```

Nonlinear Elastic Analysis:

```
b=55.2748 ! Deformation for P = 100psi
[28]
/prep7
csys,0
ET,1,hyper56
MP,NUXY,1,0.49
TB,MOONEY,1,2
TBDATA,1,80
TBDATA,2,20
CYL4, , ,7,0,18.625,90
/pnum,line,1
lplo
LSEL,S,LINE,,1
LESIZE,ALL,,,20
LSEL,S,LINE,,3
LESIZE,ALL,,,20
LSEL,S,LINE,,2
LESIZE,ALL,,,10
LSEL,S,LINE,,4
LESIZE,ALL,,,10
allsel
amesh,1
/solu
!dl,2,,symm
!dl,4,,symm
ANTYPE,STATIC
NLGEOM,1
NSUBST,71,80,70
LNSRCH,0
NEQIT,100
pred,off
/FORMAT,,,20,14
lsel,s,line,,1,4
nsll,s,1
*get,numloop,NODE,0,count
*do,i,1,numloop
*get,nodeload,NODE,NN,NXTH
*get,Yloc,NODE,nodeload,loc,Y
```

```
*get,Xloc,NODE,nodeload,loc,X
R=sqrt(Xloc**2+Yloc**2)
costheta = Xloc/R
sintheta = Yloc/R
Ur=-R+sqrt(R**2+b)
DeX= Ur*costheta
DeY= Ur*sintheta
d,nodeload,ux,DeX
d,nodeload,uy,DeY
NN=nodeload
*enddo
allsel
solve
/post1
rsys,1
nsel,s,,,42
!prnsolms
!Svon=19.02982139587
allsel
plnsol,s,eqv
```

3. A Plate in Uniform Plane Strain

Linear Elastic Analysis:

```
b=100
h=200
EZ=70
PL=0.1
/prep7
et,1,plane42
ex,1,70
keyopt,1,3,2
nuxy,1,0.499
k,1,
k,2,100
k,3,100,200
k,4,,200
l,1,2
l,2,3
l,3,4
l,4,1
lplo
al,1,2,3,4
aplo
esize,20
amesh,1
/pnum,nodes,1
eplo
/solu
NN=0
Nu= 0.5
lsel,s,line,,1,4
aplo
nsll,s,1
*get,numloop,NODE,0,count
*do,i,1,numloop
*get,nodeload,NODE,NN,NXTH
*get,xloc,NODE,nodeload,loc,x
DeX=(-PL*(1-Nu**2)/EZ)*(xloc-(b/2))
d,nodeload,ux,DeX
NN=nodeload
*enddo
NN=0
*get,numloop,NODE,0,count
*do,i,1,numloop
*get,nodeload,NODE,NN,NXTH
*get,Yloc,NODE,nodeload,loc,Y
DeY=(PL*Nu*(1+Nu)/EZ)*(yloc-(h/2))
d,nodeload,uy,DeY
NN=nodeload
*enddo
allsel
/FORMAT,,,20,14
Solve
/post1
plnsol,s,x
```

Nonlinear Elastic Analysis:

```
!Nonlinear deformation - external pressure = 1000 Pa
/prep7
ET,1,HYPER56
MP,NUXY,1,0.499
TB,MOONEY,1,5
TBDATA,1,260
TBDATA,2,80
TBDATA,3,3940
TBDATA,4,-4060
TBDATA,5,1070
k,1,
k,2,100
k,3,100,200
k,4,,200
l,1,2
l,2,3
l,3,4
l,4,1
lplo
al,1,2,3,4
aplo
LSEL,S,LINE,,1
LESIZE,ALL,,,6
LSEL,S,LINE,,2
LESIZE,ALL,,,10
LSEL,S,LINE,,3
LESIZE,ALL,,,6
LSEL,S,LINE,,4
LESIZE,ALL,,,10
amesh,1
/pnum,nodes,0
eplo
/solu
nsel,s,node,,51,59
d,all,ux
nsel,s,node,,28,73,9
d,all,uy
*dim,dx,,32   ! Arrays consisting of the boundary displacement values obtained by.
*dim,dy,,32   ! solving the problem using pressure boundary conditions
! Displacement values are not shown
lsel,s,line,,1,4
nsll,s,1
NN=0
*get,numloop,NODE,0,count
*do,i,1,numloop
```

```
*get,nodeload,NODE,NN,NXTH
        d,nodeload,ux,dx(i)*aa(i)
        NN=nodeload
*enddo
NN=0
*get,numloop,NODE,0,count
*do,i,1,numloop
        *get,nodeload,NODE,NN,NXTH
        d,nodeload,uy,dy(i)*aa(i)
        NN=nodeload
*enddo
allsel
```

```
/FORMAT,,,20,14
ANTYPE,STATIC
NLGEOM,1
NSUBST,20,21,19
LNSRCH,0
NEQIT,100
pred,off
ddele,29,ux
f,29,fx,1000
Solve
/post1
plnsol,s,eqv
```

4. Cook's Membrane

Linear Elastic Analysis:

```
/prep7
ET,1,PLANE42
keyopt,1,3,2
MP,EX,1,6*(260+80)
MP,NUXY,1,0.49
k,1,
k,2,,44
k,3,48,60
k,4,48,44
l,1,2
l,2,3
l,3,4
l,4,1
lplo
al,1,2,3,4
aplo
LSEL,S,LINE,,1,3
LESIZE,ALL,,,10
LSEL,S,LINE,,2,4
LESIZE,ALL,,,10
allsel
amesh,1
/solu
lsel,s,line,,1,4
nsll,s,1
aplo
nsll,s,1
```

```
*dim,dx,,40 ! arrays of displacement values obtained by solving the problem with
*dim,dy,,40 !pressure boundary conditions
dx(1)=0,0,0,0,0,0,0,0
dx(9)=0,0,0,-3.2848,-0.2712,-0.56817,-0.81515,-1.1089
dx(17)=-1.4087,-1.741,-2.0857,-2.4522,-2.8369,-1.0252,-2.9722,-2.6953
dX(25)=-2.4448,-2.2125,-1.997,-1.7922,-1.5979,-1.4081,-1.2199,-0.50029
dx(33)=-0.13405,8.95E-02,0.19749,0.20609,0.15165,7.69E-02,2.55E-02,5.90E-03
dy(1)=0,0,0,0,0,0,0,0
dy(9)=0,0,0,4.2176,0.26427,0.34927,0.56849,0.8131
dy(17)=1.1482,1.5555,2.0521,2.6405,3.3095,4.0985,4.2226,4.2101
dy(25)=4.1926,4.1697,4.1482,4.126,4.1079,4.0939,4.0884,3.3031
dy(33)=2.5876,1.9574,1.4334,1.0181,0.71458,0.50404,0.34289,0.18077
*get,numloop,NODE,0,count
*do,i,1,numloop
        *get,nodeload,NODE,NN,NXTH
        *get,xloc,NODE,nodeload,loc,x
        d,nodeload,ux,dx(i)
        NN=nodeload
*enddo
NN=0
*get,numloop,NODE,0,count
*do,i,1,numloop
        *get,nodeload,NODE,NN,NXTH
        *get,Yloc,NODE,nodeload,loc,Y
        d,nodeload,uy,dy(i)
        NN=nodeload
*enddo
allsel
/FORMAT,,,12,5
solve
/post1
prnsolms
plnsol,s,eqv
pldisp,2
```

Nonlinear Elastic Analysis

```
/prep7
ET,1,HYPER56
MP,NUXY,1,0.4999
TB,MOONEY,1,5
TBDATA,1,260
TBDATA,2,80
TBDATA,3,3940
```

```
TBDATA,4,-4060
TBDATA,5,1070
k,1,
k,2,,44
k,3,48,60
k,4,48,44
l,1,2
l,2,3
l,3,4
l,4,1
lplo
al,1,2,3,4
aplo
LSEL,S,LINE,,1,3
LESIZE,ALL,,,10
LSEL,S,LINE,,2,4
LESIZE,ALL,,,10
allsel
amesh,1
/solu
lsel,s,line,,1,4
nsll,s,1
aplo
nsll,s,1
*dim,dx,,40 ! arrays of displacement values obtained by solving the problem with
*dim,dy,,40 !pressure boundary conditions
dx(1)=0,0,0,0,0,0,0,0
dx(9)=0,0,0,-35.889,-4.8061,-7.7221,-10.625,-13.713
dx(17)=-16.982,-20.445,-24.042,-27.818,-31.741,-26.291,-34.955,-33.973
dx(25)=-32.994,-32.009,-31.038,-30.062,-29.101,-28.149,-27.208,-20.672
dx(33)=-15.308,-10.118,-5.3708,-1.8443,-6.73E-02,0.30786,0.13476,2.97E-02
dy(1)=0,0,0,0,0,0,0,0
dy(9)=0,0,0,47.091,4.3441,6.4122,10.498,14.401
dy(17)=19.025,23.913,29.16,34.693,40.511,49.896,47.303,47.729
dy(25)=48.134,48.489,48.791,49.046,49.258,49.446,49.636,43.692
dy(33)=37.955,32.25,26.455,20.651,15.248,10.62,6.6847,3.0993
*get,numloop,NODE,0,count
*do,i,1,numloop
        *get,nodeload,NODE,NN,NXTH
        *get,xloc,NODE,nodeload,loc,x
        d,nodeload,ux,dx(i)
        NN=nodeload
*enddo
NN=0
*get,numloop,NODE,0,count
*do,i,1,numloop
```

```
        *get,nodeload,NODE,NN,NXTH
        *get,Yloc,NODE,nodeload,loc,Y
        d,nodeload,uy,dy(i)
        NN=nodeload
*enddo
allsel
ANTYPE,STATIC
NLGEOM,1
NSUBST,100,101,99
LNSRCH,1
NEQIT,1000
pred,off
/FORMAT,,,12,5
solve
/post1
prnsolms
plnsol,s,eqv
pldisp,2
```